

Surface-Confined Supramolecular Coordination Chemistry

Nian Lin¹ (✉) · Sebastian Stepanow² (✉) · Mario Ruben³ (✉) ·
Johannes V. Barth^{4,5} (✉)

¹Department of Physics, The Hong Kong University of Science and Technology,
Clear Water Bay, Hong Kong, P.R. China
phnlin@ust.hk

²Centre d'Investigacions en Nanociència i Nanotecnologia (CIN2-ICN), UAB Campus,
08193 Bellaterra, Spain
sebastian.stepanow.ICN@uab.es

³Institut für Nanotechnologie, Karlsruhe Institute of Technology, P.O. Box 3640,
76021 Karlsruhe, Germany
mario.ruben@int.fzk.de

⁴Physik Department E20, Technische Universität München, James Franck Str.,
85748 Garching, Germany

⁵Department of Physics & Astronomy – AMPEL, The University of British Columbia,
2355 East Mall, Vancouver, V6T 1Z4, Canada
jvb@ph.tum.de

1 Introduction

2 Concepts

3 In vacuo Metallosupramolecular Engineering at Solid Surfaces

3.1 Principles

3.2 STM Observations

3.3 Computational Modeling

4 Metal Ion–Ligand Assemblies at the Solid–Liquid Interface

5 Résumé and Perspectives

References

Abstract The non-covalent synthesis of coordination compounds and networks provides promising avenues towards metal-containing supermolecules and nanostructured materials with ultimate feature definition. An important factor for their further development, and their integration and exploitation in nanoscale functional systems, is the capability to prepare or organize them at well-defined substrates or templated environments. Supramolecular engineering on atomistically controlled surfaces has been propelled by the direct insight into low-dimensional coordination systems provided by scanning tunneling microscopy observations. Here we discuss the principles of *surface-confined supramolecular coordination chemistry*, emphasizing self-assembly protocols conducted on surface atomic lattices employing metal centers to direct the organization of molecular ligands and the template-induced organization of prefabricated metallosupramolecular species. The presented exemplary molecular-level studies elucidate the arrangement of organic

adsorbates and transition metal adatoms on low-index metal and graphite surfaces. They reveal the interplay between molecule–adatom, intermolecular, and adsorbate–substrate interactions, which need to be balanced for the fabrication of low-dimensional nanostructures. The control and understanding of both the nature of metal–ligand interactions and the resulting supramolecular organization on solid surfaces is decisive for the design of advanced architectures with concomitant functions. The realized metallosupramolecular compounds and arrays combine the properties of their constituent metal ions and organic ligands, and feature versatile structural characteristics as well as attractive functional aspects: their redox, magnetic, spin-state, and electronic transitions.

Keywords Interface science · Metal surfaces · Metal-directed assembly · Scanning tunneling microscopy · Supramolecular engineering · Surface coordination chemistry

1

Introduction

The foundations of coordination chemistry were laid in 1892 by Werner, who expounded in a landmark publication the constitution of inorganic compounds where metal centers are surrounded by a specific number of ligands in a symmetrical geometric arrangement [1]. He notably introduced the concept of *Hauptvalenz* and *Nebenvaleanz* for metal ions and analyzed the isomerism of optically active complexes [2]. This eventually led to the acceptance of his views, that were confirmed by X-ray diffraction studies [3, 4]. Their description in terms of quantum mechanical modeling led to the formulation of ligand field theory [5–7]. At the same time, the intriguing magnetic properties of the metal centers in different environments were analyzed [8, 9]. In the following decades the science of coordination compounds became a mature research field and independent chemistry discipline [10, 11].

On the other hand, the first systematic surface science investigations were conducted in the 1910–1920s, notably focusing on phenomena like chemisorption, diffusion of adsorbed species, heterogenous catalytic reactions, growth of thin films or thermionic electron emission [12–26], and the “life history of adsorbed atoms and ions”, dubbed adatoms [27]. Important feats were the derivation of the Langmuir isotherm relating the concentration of adsorbed molecules on a solid surface to their gas phase pressure at fixed temperature – named after the leading surface chemist of the time who formulated it [12]; and the first demonstration of electron diffraction from a crystal surface [28], which was equally important in proving the electron’s wave nature and in the later development of a major surface science tool, low-energy electron diffraction [29, 30].

Coordination and surface chemistry represent scientific movements with rather disparate origins and accordingly there was hardly any crosstalk during their initial development. The situation changed when in the 1960s the era of *modern surface science* was entered, triggered by the widespread availability of ultra-high vacuum systems and the development of sensitive tools for the structural and chemical characterization of solid surfaces and adsorbates thereon [31]. This notably led to an improved understanding regarding the bonding and chemical reactions of molecular ligands on metals [32, 33]. Based on the experimental evidence, analogies between coordination chemistry and surface chemical bond formation and reactions were delineated [34–41]. This relation between the chemistry of adsorbates on metals and coordination compounds is expressed in the term *surface coordination chemistry*. Similar considerations hold regarding the surfaces of metal oxide catalysts, where surface atoms are characterized by a ligand sphere differing from that in the bulk, whence the metal centers have reduced coordination numbers and can be designated *coordinatively unsaturated sites* (abbreviated *cus*) [42]. Their coordination sphere may be completed by adsorbed molecular species, and these may be activated for catalytic transformations [43–47]. Thus there is an analogy between surface processes on oxides and those occurring in homogenous catalytic reactions mediated by metal complexes in both natural and synthetic metal-containing systems [48, 49]. The derived *surface organometallic chemistry* [48], aiming at the rational design of single-site heterogeneous catalysts by anchoring catalytically active complexes on surfaces to achieve novel reaction pathways bears much promise [50–52], also in view of its potential to eventually mimic the function of metallobiomolecules [53–56]. Further recent applications of surface coordination chemistry encompass the control of superconductor surfaces [57], corrosion inhibition [58], the magnetochemistry of nanoparticles [59], as well as the anchoring of functional metal–organic species on Si surfaces [60–62] and – last but not least – on titanium oxide nanoparticles as dyes for photovoltaic cells [63].

During the 1980s the chemistry of large supermolecules and networks stabilized by metal–ligand interactions moved, at least partially, under the auspices of supramolecular science [64, 65]. Thus supramolecular coordination (or metallosupramolecular) chemistry evolved, relying on the paradigms of molecular recognition and metal-directed assembly, which represent a key strategy for the engineering of highly organized systems using discrete molecular building blocks (sometimes designated *tectons*). The intense research efforts revealed tremendous potential in the areas of catalysis, molecular electronics, molecular magnetism, sensor design, and optics [66]. The use of metal ions offers a set of directional bonds of intermediate strength that is exploited to realize distinct geometric shapes. Supramolecular coordination chemistry has gathered a vast database of metal–ligand pairs with a huge variety of specific binding schemes giving the possibility to program selectivity

and directionality directly into the binding motif. This allows for the self-assembly of supramolecular architectures as diverse as polygonal clusters, polyhedra, cages, and grids [64, 67–72]. Moreover, the synthesis of highly porous solid frameworks and coordination polymers has reached a mature level [73–81]. Therefore, the use of transition metal centers, or in general secondary building blocks, and coordination chemistry for directing the formation of complex structures has evolved into one of the most widely used strategies for organizing molecular building blocks into supramolecular arrays. The formation of a given supramolecular shape is driven by the inherent symmetry of the available metal orbitals and the spatial organization of the donor atoms in the organic ligand system. Therefore, careful consideration must be given to the preferred coordination environment of the metal to be used and the binding mode of the linkers, in particular chelating ligands. Given such a coordination environment around the metal centers, the symmetric and rigid extension of the ligand system from mono- to multitopicity will automatically lead to a infinite grid-like one-, two-, or three-dimensional coordination network with regularly arrayed metal ions. The supramolecular organization is encoded in the electronic structure of both the metal ions and in the organic ligands. The interpretation of this information during the self-assembly process leads to a mutually acceptable structure. The principle of using metals with predetermined coordination numbers and angles as building blocks and functional units is not only an appealing method from the synthetic chemistry point of view. The transition metal ions incorporated into such structures do not merely act as stabilizing agents of the structures but remain accessible for the construction of more complex structures [82], featuring modular, hierarchic, or even dynamic behavior. Furthermore, they possess multiple electronic/spin states and a related variety of redox, photochemical, and magnetic properties, which can be tuned by the specific coordination environment. Thus the potential applications of these complex systems lie in the scientific fields of chemistry, biology, and materials science, including, e.g., catalysis, sensing, and construction of various devices on the molecular level [83–85].

In parallel, modern surface science was revolutionized over the years following the introduction of scanning tunneling microscopy (STM) in the early 1980s [86]. STM and related techniques proved to be extremely versatile tools for the direct observation of surface phenomena. Moreover, the controlled manipulation of individual adsorbed species to write at the atomic scale or create quantum confinement structures symbolized the striking advance and highlighted the promise of nanoscale science and technology [87, 88]. While many research groups explored single-molecule chemistry experiments [89–92], molecular-level nanoscience simultaneously provided the basis to explore concepts from supramolecular chemistry for the fabrication of molecular architectures on well-defined planar substrates [93–97]. It became clear that surfaces represent unique platforms on which a novel 2D supra-

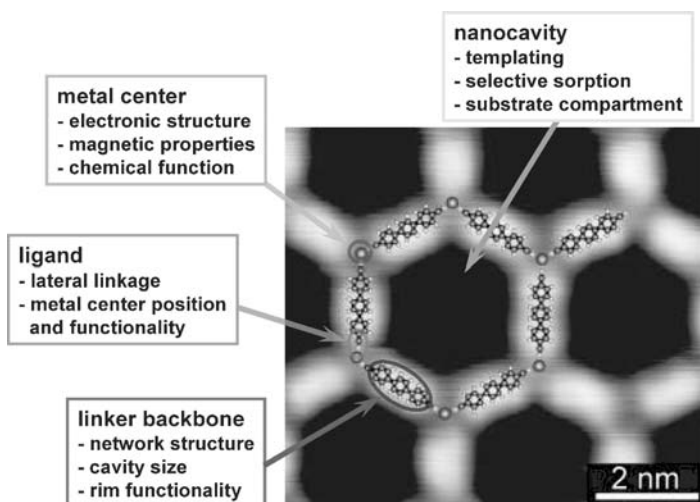
molecular chemistry can be explored to realize distinct low-dimensional molecular arrangements employing adsorbed molecules with functionalities for selective non-covalent interactions, mediated by polar exodentate moieties [98–100], hydrogen bonding groups [101–105] or zwitterionicity [106]. In addition, the significant potential of surface-confined supramolecular coordination chemistry emerged [94, 95, 107–124], as detailed in the following section.

2 Concepts

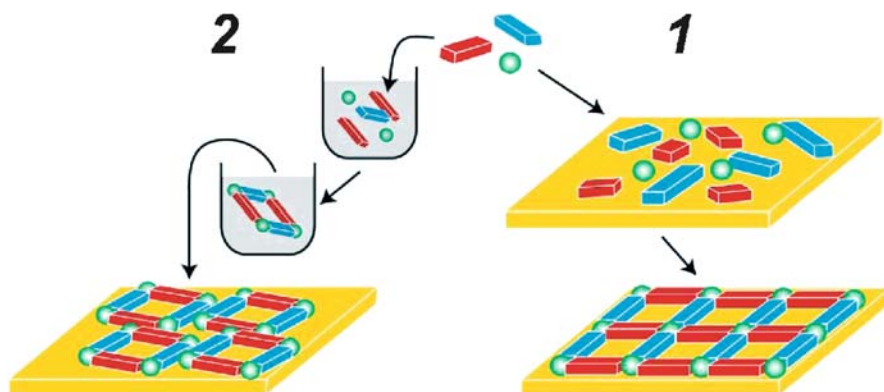
In the present context it is important to fully appreciate that a molecule's spatial confinement imposes steric constraints for molecular recognition and that the coupling of the adsorbates to the surface plays a role of comparable importance with that of the non-covalent bonds typical of supramolecular complexes, and even may entirely dominate the investigated systems [123]. Thus, one demands the development of a conceptual framework for using the surface as an assistance to guide metal-directed self-assembly processes, i.e., to address the concomitant positioning of molecules with surface-adapted functional units and metal centers. Such a scheme is similarly of interest for the deposition of pre-assembled metallosupramolecular entities. Moreover, the surface plays an important role regarding the functional properties of the low-dimensional coordination systems it supports. In particular, the properties of transition metal centers embedded in the organic layer can be affected by the intricate interplay between the present interactions, e.g., the substrate electrons can influence their magnetic moments [125–127]. The balance between metal–ligand, intermolecular, and surface interactions assumes therefore a critical role in determining the chemical and electronic properties of supramolecular layers [123, 128]. At the same time, the adsorbed ligand's chemical state [104, 129–131] and conformation [132–140] need to be assessed because they affect both the functional properties and organizational behavior of adsorbed molecular nanosystems.

The control and fabrication of single compounds, and the organization of metal–organic units in 1D coordination polymers or 2D coordination arrays is of interest in metallosupramolecular engineering on surfaces. The key features and their role in the potential functionality of the particularly versatile nanoporous networks achieved by metal-directed assembly in vacuum are illustrated in Scheme 1. The work on the formation of supramolecular architectures on surfaces containing metal centers will here be divided into the two approaches illustrated in Scheme 2.

1. On the one hand, the ultra-high vacuum (UHV) approach has been pioneered over the last decade because of its exquisite surface control and



Scheme 1



Scheme 2

cleanness rendering submolecular level resolution in scanning tunneling microscopy (STM) imaging. By using the UHV approach, the assembly process of metallosupramolecular architectures can be directly conducted following the deposition of the components, i.e., organic linkers and metal atoms (Scheme 2, right). For the realization of low-dimensional coordination systems one has to take care about the different mobility characteristics of the adsorbates, i.e., organic molecules and metal adatoms, which can differ by several orders of magnitudes [123, 141–143]. Apart from the non-covalent lateral interactions between the adsorbates, there can be strong and irreversible interactions with the surface, e.g., the alloying of metal adatoms [144–148] or chemical reactions of the organic species with the surface that alter their chemical state [104, 129–131]. The point of in-

terest for their potential functional properties in the 2D metal–organic architectures are their versatile structural characteristics with the common feature of metal centers [149, 150]. STM studies of organic building blocks adsorbed on metal surfaces revealed that their supramolecular ordering is governed by the competition of intermolecular hydrogen, π – π -, van der Waals interactions, and dipolar bonds with site-selective substrate bonding. As a consequence of the linker’s surface confinement, also with metal centers employed as steering agents, the reduction to two dimensions is quite generally accompanied by coordinatively unsaturated sites. This opens the way to realize unique compounds and study a novel class of metallosupramolecular systems. Thus, the choice of donor atoms, bridging groups, metal ions, and systematic synthetic design strategies might render these systems ideal for designing perfectly surface-adapted receptor sites with tailorable molecular recognition properties, and catalysts with tunable reactivities.

2. On the other hand, systematic studies have been performed at the solid–liquid interface and representative examples will be discussed in Sect. 4. Frequently the molecular building blocks are pre-assembled into entities stabilized themselves by metal coordination centers (see Scheme 2, left). Such so-called *supermolecules* are brought to the surface by drop-casting, spin-coating, or other methods, where they bind and form specific patterns (cf. [118, 151, 152]). The involved coordinated metal ions assure the integrity of the molecules and are not directly involved in the surface linkage of the molecules. Alternatively, layers from the ligands can be pre-organized on the surface by self-assembly or by tethering techniques and subsequently modified with the addition of metal atoms, i.e., by in-situ complexation, or by interfacial reactions in electrochemically controlled environments. A further important advantage when using a solution-based surface approach with electrochemical methods is the possibility of combined self-assembly–molecular electronics studies [153–155].

A special situation is encountered with metal–porphyrin or metal–phthalocyanine molecules that can be either deposited by sublimation under UHV conditions or in solution environments. For these macrocyclic compounds, free-base species exist, i.e., the metal centers are not required per se as a construction unit. The building of supramolecular structures that incorporate porphyrin subunits is of great interest to many research groups. The rich photochemistry and redox properties (e.g., photoinduced electron transfer, luminescence, and light harvesting) of porphyrins have driven this interest. Porphyrins or phthalocyanines have a rich coordination chemistry that allows the inclusion of many different metal centers at their macrocycle. They serve in many respects as a model system since this constitutes a low-coordination complex. Recent STM studies report on the organization of metal-coordinated or free-base porphyrins as well as phthalocyanines on

various metal surfaces. In particular, chemically modified molecules with additional functional groups as *meso*-substituents, (e.g., pyridyl or other bulky groups) were at the focus of investigation. These additional exodentate ligands play a similar role in the determination of the adlayer structure as the metal-containing macrocycle and can be used to effectively control the arrangement of the functional molecules on the surface. Such systems have also been studied for their complexation chemistry that takes place directly at the surface in vacuo. Upon exposure of free-base porphyrins to a beam of transition metal atoms, selective complexation of the porphyrin macrocycle occurs leaving the template structure preserved [156, 157]. This approach can be even employed for rare-earth centers [158]. Although the complexation reaction is not involved in the formation of the adlayer structure, the controlled in-situ metalation of adsorbed porphyrins provides a novel route toward high-purity metalloporphyrin architectures and patterned surfaces. Many aspects regarding metal–porphyrin or metal–phthalocyanine adlayer systems are discussed elsewhere (cf. [140, 159–171]; see also the review [172] and references therein) and thus not developed here in detail.

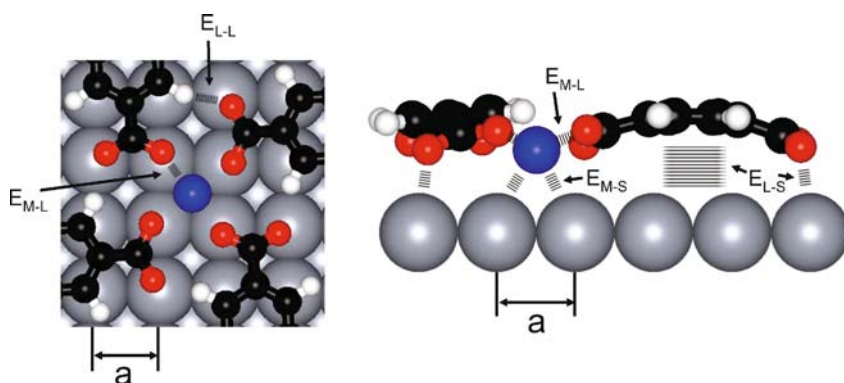
3

In vacuo Metallosupramolecular Engineering at Solid Surfaces

3.1

Principles

In this section we provide a status report on the modular assembly of metal–organic compounds, polymers, and networks using molecular linkers with aromatic backbones in UHV conditions on clean metallic surfaces, i.e., without any solvent or atmospheric molecular concomitants. Attractive interactions between aromatic bricks with the metal substrate frequently favors a flat adsorption configuration, i.e., with the ligands' π -systems parallel to the surface plane. This is illustrated in Scheme 3, that also depicts the multiple and competing interactions between adsorbed metal centers, functional molecular groups, and the substrate atoms arranged in a lattice with periodicity a . A direct consequence of the ligand's 2D confinement is that steric restrictions prevent the expression of many 3D coordination motifs. Moreover, the surface bonding of both admetal centers and organic linkers is typically at specific sites on the substrate atomic lattice (labeled E_{M-S} and E_{L-S} in Scheme 3, respectively). The easiest translational (rotational) path between two equivalent bonding sites is separated by the so-called migration (rotation) energy barrier, that can be a sizable fraction of the bonding energy [123, 141–143] and thus comes close to the energy gain from a potential coordination bond. When the site-specific bonding prevails thus only discrete configurations for

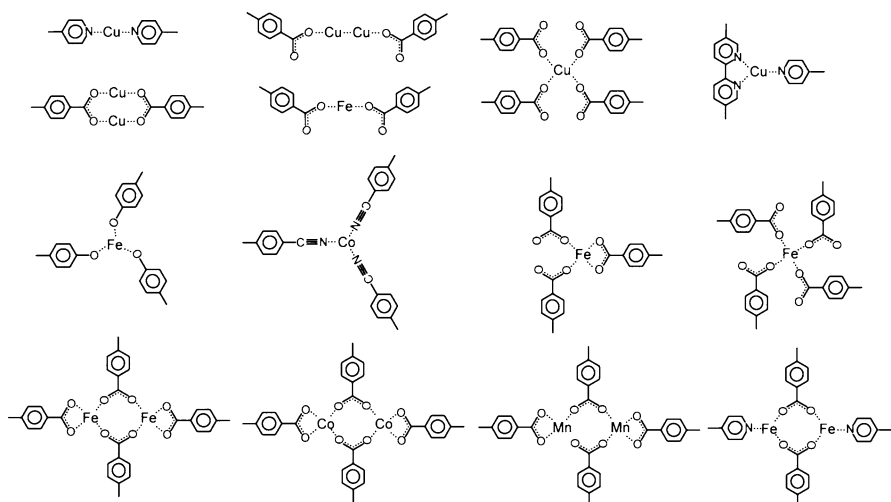


Scheme 3

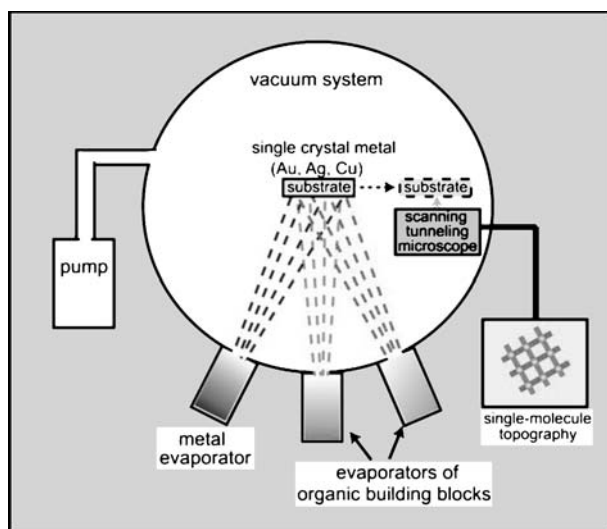
the formation of lateral bonds are possible. Consequently the metal center–ligand interactions (labeled E_{M-L}) compete with the substrate interactions (for a more detailed discussion, see [123]). In addition, their nature is affected by the modified electronic structure of the metal centers and ligands resulting from the surface chemical bonding. Furthermore, lateral interactions between the ligands (labeled E_{L-L} – for instance hydrogen bonds or substrate-mediated interactions) may play a secondary role in the 2D supramolecular organization.

The ligand functionalities explored to date include carboxylate, pyridine, hydroxyl, and carbonitrile groups. Carboxylates in particular represent a versatile class of building blocks for engineering robust 3D metal–organic frameworks or functional coordination polymers [79, 80]. One can similarly use metal–carboxylate coupling schemes on appropriate substrates to tailor coordination architectures in two dimensions. A series of systematic investigations demonstrated the construction of mononuclear metal–carboxylate clusters, polymeric coordination chains, and fully reticulated networks based on polyfunctional exodentate benzoic-acid species. These findings give insight into the principles underlying the complexation of organic ligands and transition metal centers on surfaces and illustrate their potential for rational 2D metallosupramolecular engineering. Scheme 4 shows the coordination modes that have been explored so far, and we shall discuss how the intricate interplay between the driving forces in the self-assembly process leads to specific arrangements.

A typical experimental setup is sketched in Scheme 5. Organic precursor layers are deposited on the atomically clean surfaces by sublimation of the molecular linkers, typically present in high-purity powder form. The temperature of the substrate is controllably varied from cryogenic conditions (~ 10 K) to elevated temperatures (~ 500 K) in order to achieve thermodynamically metastable or equilibrated products. In the surface-assembled systems the coordination centers are evaporated using electron beam or re-



Scheme 4



Scheme 5

sistive heating sources. The assembly conditions are set by the substrate temperature, evaporation rate or sequence, and surface concentrations of the adsorbates.

Because under vacuum conditions the sublimation of entire complexes stabilized by coordination interactions may correlate with decomposition (see [173, 174], but also note that coordinatively enhanced stability has been reported [175]), more sophisticated techniques are of interest for the handling of thermolabile species, such as pulse-deposition or electro spray methods

where fragile compounds are directly released into vacuum [176–183]. Notably, a straightforward combination of solution-based supramolecular self-assembly techniques with UHV-based STM imaging by means of pulse injection onto an Au(111) surface was the key for the successful observation of ring-like molecular structures containing up to 30 Zn^{II} metal ions and exhibiting an internal diameter of ~ 10 nm [184].

3.2

STM Observations

A direct illustration of the capturing of transition metal centers by the terminal pyridyl groups of a surface anchored porphyrin species is provided by the experiment depicted in Fig. 1 [138]. The isolated tetra-pyridyl-porphyrin (TPyP) molecules are immobile following adsorption on a Cu(111) substrate at 300 K. Single Fe atoms were added in situ at 8 K, where thermal diffusion is frozen. Figure 1a accordingly shows randomly distributed Fe monomers appearing as round protrusions coexisting with TPyP. In a next step, the sample temperature was slightly increased to about 15 K, which allows the Fe adatoms to freely migrate on the surface, while the TPyP remains stationary. Subsequently, the sample was cooled down again. As a result, Fe is selectively captured by the pyridyl groups (Fig. 1b). Once attached the adatoms stick, whereby the modified imaging characteristics of both Fe and TPyP-endgroups indicate marked chemical interaction. These findings confirm that the N-containing ligands retain their affinity towards metal centers despite the simultaneously observed conformational adaptation of the porphyrin unit, implying a non-planar orientation of pyridyl groups.

The measurements visualize the impact of metal–ligand interactions and a metallosupramolecular self-assembly process in two dimensions, where the

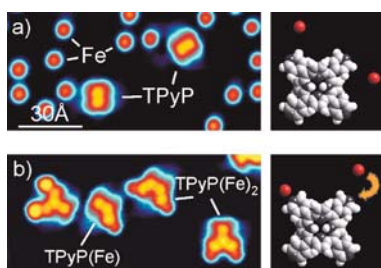


Fig. 1 Selective attachment of Fe adatoms to the pyridyl groups of TPyP adsorbed on Cu(111) (images are of identical size). The porphyrin species is immobile following deposition at 300 K. **a** Upon codeposition of Fe at very low temperatures ($T = 8$ K), there is a random distribution of Fe monomers. They become mobile at $T = 15$ K and are irreversibly attached to the pyridyl ligands of the porphyrins (**b**). Two main steps of this experiment are schematically illustrated in the column on the right. Adapted from [138]

organic linkers are spatially anchored. Furthermore, additional incoming Fe monomers can be trapped by the metal–ligand complex, resulting in small metal clusters pinned to the pyridyl groups of the TPYP (Fig. 1b, complex on the left). Such changes could be equally achieved by single atom manipulation experiments, i.e., by positioning Fe atoms at the pyridine ligands with the STM tip [168]. In a related manipulation experiment, the bonding between a single Au atom and pentacene molecules was induced [185]. At higher temperatures, where surface adatoms are supplied from step edges and the TPYP molecules become mobile, pairing and chaining of TPYP is encountered, mediated by Cu-directed coupling of the pyridyl endgroups [186]. Surprisingly, the pairing of two molecules interconnected with just one metal–organic linkage strongly increases the mobility of the dimers formed, i.e., their diffusion rates exceed those of monomers by more than one order of magnitude. Furthermore, indications exist that the Cu adatom dimers can also mediate the coupling of the pyridine ligands [186]. Such pairs were similarly identified in the structure-determining element of 2D metal–organic oligopyridine networks recently realized on a graphite substrate [187]. The copper–nitrogen affinity was also exploited to create coordination dumbbells in Cu-directed assembly of mixed bipyridine and pyridyl linkers [188]. Moreover a tetraazaperopyrene on Cu(111) was used to realize a porous network where the dye molecules coordinate to Cu adatoms through their N atom lone pairs in a cyclic arrangement [189]. In this case the coordination network could even be employed as a precursor structure to mediate the formation of covalent bonds following thermal annealing.

In a different reaction scheme, one can take advantage of the functional porphyrin macrocycle to create metalloporphyrin compounds and nanoarchitectures in 2D. Upon exposure of regular TPYP arrays self-assembled on Ag(111) to iron monomers supplied by an atomic beam, selective complexation occurs whereby the template structure is strictly preserved [156]. This expands the diversity of metalloporphyrin layers conventionally realized by evaporation of integral species, because in-situ metalation provides a route towards novel metalloporphyrin nanoarchitectures and patterned surfaces [156–158]. In a related reaction pathway, evidence could be obtained for in-situ complexation and metal center-induced switching of phenanthroline-based catenane units deposited the Ag(111) surface [182].

Early evidence of lateral metal–ligand bonding in molecular systems at vacuum–solid interfaces was found for low-coverage benzoic acid adlayers on Cu(110) [190–192]. The proposed model contained two Cu adatoms bridging two opposing benzoate moieties. In this study it was concluded that the Cu adatoms play a specific role for the adsorption geometry of the molecules, where the π -interaction of the aromatic backbone favors a flat geometry and the carboxylate group favors an upright configuration. The necessary deprotonation of the acid group is thermally activated on the Cu surface. The reaction is partially accompanied by the formation of upright species.

The same mechanism for the formation of molecular pairs at elevated temperatures (425 K) was proposed for 4-[*trans*-2-(pyrid-4-ylvinyl)]benzoic acid (PVBA) adsorbed on Cu(111) (see Fig. 2a) [94]. The Cu adatoms are provided by the continuous evaporation/condensation from the surface atomic steps [193]. The rate of detachment from the kink sites on the terraces on Cu(111) is lower than on Cu(110), which is the reason for the requirements of thermal activation for the complex formation in the case of PVBA compared to the benzoate structures mentioned above. By comparison, on the less reactive Ag(110) substrate no similar compounds evolve; however, there is a reshaping of the substrate steps induced by the functional carboxylate group [194].

The first unambiguous identification of distinct metal–organic coordination complexes formed on a surface was demonstrated by the Cu-TMA (1,3,5-benzoic tricarboxylic acid) system. Two types of complexes, $\text{Cu}(\text{TMA})_4$ and $\text{Cu}_2(\text{TMA})_6$ were observed when TMA molecules were deposited on Cu(100) (Fig. 2b). Again, the metal centers are provided by the Cu substrate via thermally activated step evaporation. The energetics of the surface chemical processes permits monitoring of the metal–ligand bonding by STM imaging. For instance, the complexation reaction of clover-leaf shaped $\text{Cu}(\text{TMA})_4$ enti-

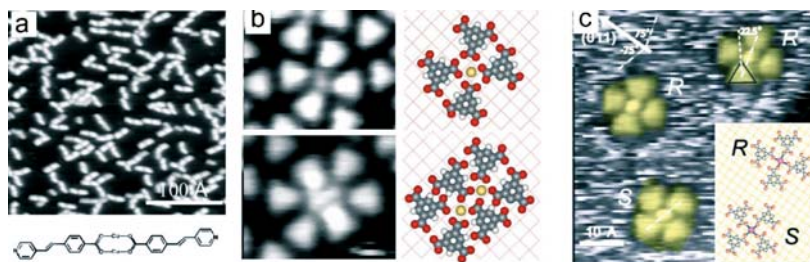


Fig. 2 Metal–carboxylate compounds on copper surfaces. **a** Pairing of PVBA molecules upon deposition on Cu(111) at elevated temperatures (adsorption at 425 K, imaged at 77 K). The corresponding tentative model shows the copper–carboxylate bonding with a head-to-head coupling of two PVBA molecules. **b** STM topographs and corresponding models of trimesic acid–copper complexes spontaneously assembling on Cu(100) at 300 K. The molecules’ triangular shape reflects a flat-lying adsorption geometry. The *upper panel* shows a cloverleaf-shaped arrangement of four TMA molecules with a central Cu adatom protrusion. The *lower panel* depicts a STM image and model of the Cu_2TMA_6 coordination compound with four unidentate and two *syn,syn* coordination bonds. **c** High-resolution image showing the two FeTMA_4 stereoisomers on the Cu(100) surface, labeled *R* and *S*, representing mirror-symmetric species with respect to the [011] substrate direction. The corresponding model depicts a unidentate coordination of the carboxylate ligands to the central Fe atom (placed on the hollow site) with a bond length of about 2 Å (solid lines). The corresponding rotation of the carbon backbone is strictly correlated for all TMA molecules in a given complex. The resulting symmetry break accounts for the chirality of the complexes. Adapted from [94, 110, 111]

ties allows one to gain quantitative information of the formation, energetics, and dynamics of individual complexes on Cu(100) [110]. Notably the energy barrier for the 2D dissociation reactions was determined to be 0.31 eV. The lifetime of the complexes increases significantly when stabilized by the surroundings being either other molecules or surface step edges. Besides being engaged in the complexation, the Cu adatoms are simultaneously potential agents for the deprotonation of the carboxylic moieties [195]. At low temperatures where the deprotonation reaction is inhibited, stable hydrogen-bonded networks are observed whereas at elevated temperatures metal-organic arrangements evolve due to the catalytic activity of the substrate [129]. To verify this concept it was shown that TMA molecules adsorbed on a Ag(111) surface do not undergo deprotonation reactions at ambient temperatures [195], whereas at elevated temperatures [196] or in the presence of Cu adatoms made available by codeposition the reactive carboxylate linkers evolve.

The Cu-TMA complexes described above are intrinsically 0D entities because they do not organize as extended metal-organic arrays. In order to realize compounds where the supply of all constituents is controlled by the experimentalist, the coordination interaction of TMA with Fe adatom centers was probed (Fig. 2c) [111]. The iron was codeposited at low temperatures in order to inhibit intermixing reactions with the surface. The resulting complexes appear exclusively in the presence of Fe on the surface and are distinct from their Cu-based counterparts, notably featuring reduced bonding distances and 2D chirality. The STM observations at room temperature reveal two mirror-symmetric square-planar $\text{Fe}(\text{TMA})_4$ complexes where the correlated attachment of the ligands defines the handedness of the entity. In contrast to the Cu-TMA cloverleaves, isolated Fe complexes are thermally stable at 300 K. Upon annealing the surface decorated with $\text{Fe}(\text{TMA})_4$ complexes to 350 K, they aggregate in a 4×4 grid pattern comprising 16 TMA and 9 Fe [114]. These grid-like structures inherit the chiral nature of the central $\text{Fe}(\text{TMA})_4$ complexes and are randomly distributed at the surface (vide infra).

In subsequent systematic investigation it was shown that by employing the symmetric linker 1,4-benzoic dicarboxylic acid (terephthalic acid, TPA), the linear analogue of TMA, one can achieve distinct regular 2D structures consisting of coordination complexes interconnected by hydrogen bonds on a Cu(100) surface in the low Fe concentration regime [197]. The molecules form mononuclear iron complexes $\text{Fe}(\text{TPA})_4$ where four molecules coordinate each with one carboxylate oxygen to the Fe center, and the ligands assume two different mirror symmetric senses of rotations around the Fe center. The individual Fe centers span a (6×6) -superstructure commensurate with the Cu(100) lattice (Fig. 3a), and this square array extends over entire substrate terraces. The high degree of long-range organization is presumably mediated by secondary intercomplex carboxylate-phenyl hydrogen bonds (see model in Fig. 3b). This rather unusual hydrogen bond has been identified in related adlayer systems [130, 131, 198, 199] and analyzed by theoretical means [196].

It represents a particular member of the class of ionic hydrogen bonds [200]. A domain of complexes contains only one type of handedness signaling the chiroselectivity of the intercomplex interaction. The lower-symmetry derivative 1,3,4-benzoic tricarboxylic acid (trimellitic acid, TMLA) forms isomorphological structures, i.e., the remaining carboxylate side group of the TMLA molecule is not directly involved in the network formation [201].

At intermediate Fe concentrations for both TPA and TMLA, 1D ladder structures can be realized comprising rows of coordinated molecules along the $[011]$ or $[0\bar{1}1]$ substrate directions (Fig. 3c,d) [113, 197]. The ligands binding laterally to the rows and either bridge directly two coordination centers or interdigitate and presumably form hydrogen bonds. The number of the two different links accounts for the Fe–ligand concentration ratio present in the self-assembled structure. This suggests that the formation of true coordination bonds, as confirmed recently by X-ray photoemission measurements of oxygen and iron electronic core levels in such systems [202]. Each Fe center is coordinated to three ligands in a distorted square-planar geometry. Also, this structure is commensurate to the underlying substrate atomic lattice.

The formation of 1D structures was deliberately steered through two strategies: (i) applying anisotropic surfaces and (ii) utilizing linear coordination modes. An example illustrating the first strategy is shown by depositing TMA molecules on an anisotropic Cu(110) surface [203]. Despite the triangular arrangement of the reactive carboxylate linker moieties, which

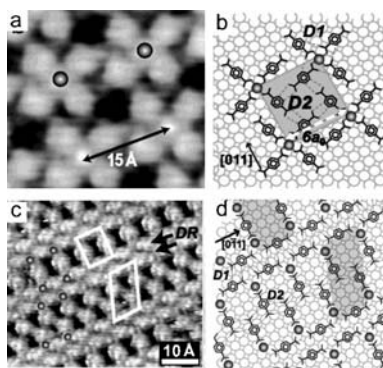


Fig. 3 Arrays of mononuclear Fe–carboxylate compounds and coordination polymers. **a** High-resolution STM image of the FeTPA cloverleaf phase on Cu(100). **b** Geometrical model of the coordination structure shown in **a**. Each Fe atom (*gray spheres*) coordinates four carboxylate ligands unidentately in a square-planar configuration. Lateral potential C–H···O hydrogen bonds are indicated. The distances $D1 = D2$ amount to 3.5 \AA . The $15 \times 15 \text{ \AA}^2$ superstructure unit cell is shown as a *gray square*. **c** STM image of the FeTPA ladder phase on Cu(100). The Fe atoms are marked by *gray spheres* and a double row by *DR*. **d** Geometrical model of **c**. *Dashed lines* indicate potential C–H···O hydrogen bonds. $D1 = D2 = 3.0 \text{ \AA}$. Adapted from [27]

would favor 2D assemblies, the molecules form 1D strings, demonstrating the strong templating effect of the substrate. The intermolecular interactions are overcome by the strong coupling to the substrate, effectively controlling the 1D character. Again mobile Cu adatoms are found to link adjacent TMA molecules along the close-packed $[1\bar{1}0]$ direction. Notably, it was shown by DFT calculations that the misleading and tempting single protrusion observed by STM could be modeled by a dimeric Cu center, confirming the geometric analysis of the structures. The intrinsic Cu–TMA linear nanostructures can be transformed into the Fe–TMA chains by preventing the formation of Cu–TMA complexes at low temperatures and subsequent deposition of Fe. The observed chains exhibit a shorter periodicity where only single Fe ions are found as the coordination centers (Fig. 4a). Thus the different chemical nature of the coordinating metal is reflected in the composition of the structures. A recent study follows the second strategy: two linear aromatic bipyridyl linkers were investigated on the isotropic Cu(100) surface [204]. Upon deposition on the substrate held at room temperature, chains evolve where the molecules are linked by a linear coordination motif of pyridine–Cu–pyridine (Fig. 4b). The Cu centers are not imaged, presumably due to an electronic effect (cf. [203]). The unconventional twofold coordination of Cu centers has not been observed in bulk coordination compounds. Similar chaining features were encountered in Cu-linked TPYP assemblies [186].

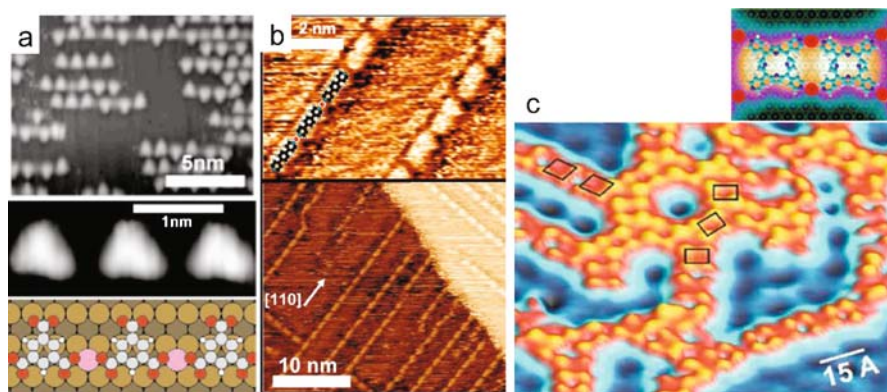


Fig. 4 Linear coordination systems. **a** STM image of Fe–TMA chains on the anisotropic Cu(110) substrate. The high-resolution topography and the corresponding model are depicted below. **b** STM images of 1,4-bis(4-pyridyl)benzene adsorbed on Cu(100) at 300 K. The structural model overlaid on the image illustrates the N–Cu–N coordination bonding. The lower STM topograph shows an overview of the chains attached to the lower side of the terrace step or running parallel on the upper side of the step. **c** Chains of self-assembled TPYP molecules on Cu(111) with the pyridyl endgroups interconnected by Cu adatoms. Individual TPYP are marked as rectangles in the large-scale image; the inset shows the coupling motif. A substrate standing wave pattern is generated by surface state electrons scattered at the metallosupramolecular strings. Adapted from [186, 203, 204]

(In this arrangement the confinement of the substrate's surface state quasi-2D electron gas moreover leads to an electron standing wave pattern at the undecorated surface areas [205]). A related chaining coordination scheme was encountered in tetracyanoethylene chains observed on the Cu(100) surface [206].

Regular 2D metal–organic coordination networks (MOCNs) were realized by the direct reticulation of coordination networks in two dimensions. In this approach distinct levels of hierarchies and complexity can be encountered. This intriguing issue, which is abundant in biological systems, was observed in Fe–TMA self-assembled layers on Cu(100) and is schematically depicted in Fig. 5a. As reported above, the TMA molecules and Fe adatoms initially form mononuclear chiral complexes at room temperature and these entities are antecedents for the higher level polynuclear 4×4 grids at evolving 350 K (Fig. 5b) [114]. At the final stage, after annealing at 400 K, the 4×4 grids are interconnected by hydrogen bonds, forming mesoscale networks comprising a regular arrangement of homochiral nanocavities. (Fig. 5c) The only control parameters in the assembly are the temperature and surface concentration. Such nanofabrication schemes involving hierarchical structures represent an

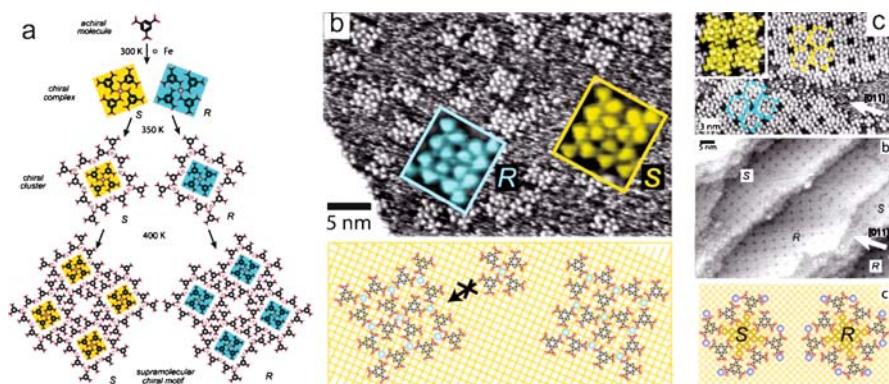


Fig. 5 *Aufbau* of dissymmetric supramolecular motifs mediated by hierarchical assembly of simple achiral species on Cu(100). **a** TMA molecules and Fe atoms represent the primary units, which are employed for the formation of secondary chiral complexes. The complexes are antecedents for tertiary polynuclear nanogrids, which are in turn the supramolecular motifs for the assembly of homochiral nanocavity arrays. The respective mirror-symmetric configurations (labeled S and R) are indicated with shaded backgrounds. **b** Assembly of tertiary stage: square-shaped polynuclear nanogrids evolve upon annealing at 350 K. The *magnified insets* and *model* below reveal that the respective core units of the dissymmetric metal–organic motifs are related to the chiral secondary FeTMA compounds. **c** Formation of extended nanocavity arrays triggered by 400 K annealing. Two homochiral domains are assembled consisting of pure enantiomers (labeled R and S), marked by *shaded rectangles*. The central opening of the domains, modeled in the *bottom panel*, is functionalized by eight surrounding carboxylate groups. Adapted from [114]

appealing possibility for the bottom-up fabrication of complex functional materials.

With both TPA and TMLA linkers, regular 2D network structures can be realized by complexation with appreciable amounts of Fe. One achieves a fully reticulated structure comprising arrays of diiron coordination centers [113, 197]. A drawback is the existence of two equivalent isomeric structures that differ in the orientation of the Fe pairs in the network nodes, i.e., they are either equally oriented or alternate as shown in Fig. 6a,b. The Fe–Fe spacing within a dimer amounts to about 4.7 Å, slightly less than twice the substrate lattice constant (2.55 Å). The coordination geometry for each Fe ion assumes a distorted square-planar geometry. Both isomeric networks reside commensurate on Cu(100) with a (6×4) and (5×5) -unit cell, respectively. These structures possess cavities of well-defined size and shape exposing the underlying Cu surface [113, 197]. Two longer analogues of TPA, 4,4'-biphenyl dicarboxylic acid (BDA) and 4,1',4',1''-terphenyl-1,4''-dicarboxylic acid (TDA), having two and three phenyl groups in the molecular backbone, respectively, form networks with increasing size similarly containing diiron centers as the essential coupling motif of the carboxylate groups (Fig. 6c,d) [115, 207]. The dimensionality dependence on the metal-to-ligand concentration ratio is absent for the longer molecules and instead coexistence of network and pure molecular domains are observed at Fe deficiency. Recently, it has been

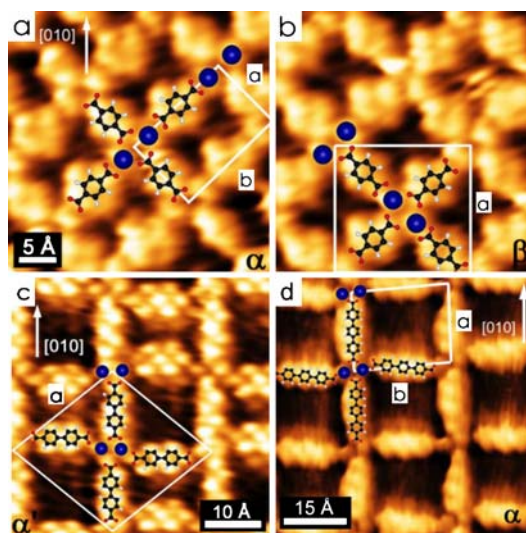


Fig. 6 Fully reticulated nanoporous Fe–carboxylate networks comprising diiron centers as coordination motif. **a,b** STM topographs of isomeric FeTPA network phases: **a** identical and **b** alternating Fe dimer arrangement. **c** High-resolution STM image of the FeBDA network. **d** STM image of the FeTDA network phase. Tentative models are superimposed on the STM images. Adapted from [207]

demonstrated that manganese–carboxylate interactions can be similarly employed to engineer 2D metal–organic lattices comprising the same dimetal centers as the Fe–carboxylate polymers and lattices presented above [208].

The replacing of the linear C–C bridge between the two aromatic rings of the BDA molecule by an ethenyl or azo group, namely 4',4''-*trans*-ethene-1,2-diyl-bisbenzoic acid and 4,4'-azobenzene dicarboxylic acid, alters significantly the appearance of the network structure. Again, the diiron coordination motif prevails [128]. But compared to the linear polybenzene dicarboxylic linkers, the network domain sizes are significantly smaller, i.e., the domains do not exceed 10 nm in size, and the structures exhibit many structural defects. Moreover, the cavity sizes and shapes span a variety of geometries and the axial orientation of the Fe pairs appears to be arbitrary. These differences can be attributed to the prochirality of the ligands, which accounts for the presence of two enantiomers on the substrate. This lack of enantioselectivity in the self-assembled structures is in contrast to the chirally resolved hydrogen-bonded pure molecular adlayers. The inclusion of both types of adsorbates in the coordination assemblies prevents the development of a perfect periodic structure that is commensurate to the Cu(100) substrate. It signals the prevailing strength of the Fe–carboxylate bond in these systems [209].

The series of the presented studies show that the carboxylate functional group frequently assumes a coordination motif with a diiron center. The carboxylate moieties are either bridging the two Fe centers or are engaged in the axial binding, being either chelating bidentate or monodentate, which also results in the evolution of isomeric phases. By replacing the symmetric linkers to dissymmetric carboxylpyridyl ligands, namely PVBA, one can eliminate the isomeric structures [210]. The carboxylate moiety acts in these system solely as an equatorial linker, whereas the pyridyl group binds strictly axially to the diiron motif resulting in a threefold coordination geometry for the metal centers. As a consequence, the orientation of the diiron centers must alternate. The realization of this structure provides the conceptual grounds that equatorial and axial ligands might be employed independently, leading to more control over the design of the network structure. Indeed, subsequent studies revealed that with the mixture of complementary carboxylate and bipyridine ligands, self-selection processes steer the size and aspect ratio of rectangular coordination networks on Cu(100), incorporating Fe centers [211].

Threefold coordination motifs, leading to such complex structures as honeycomb or kagomé lattices, are scarce in 3D compounds since low-dimensional coordination modes are less frequent. In fact, small coordination numbers were only found to occur in complexes where the steric hindrance originating from bulky ligands results in such arrangements. At surfaces, the imposed 2D confinement of the ligands and metal ions substantially influences the metal-to-ligand binding modes. In a recent study, networks

comprising trigonal mononuclear coordination nodes have been achieved by the Co- and Fe-directed assembly of ditopic dicarbonitrile- and hydroxyl-terminated polyphenyl linkers, respectively [122, 124]. This is illustrated by the hexagonal Fe-biphenolate and Co-dicarbonitrile superlattices realized on Ag(111) (Fig. 7).

The hexagonal Fe-biphenolate network could be similarly realized on the square Cu(100) substrate. The occurrence of threefold coordination motifs on substrates with different symmetries signifies that the binding motif is an intrinsic characteristic of the metal coordination and is not induced by the symmetry of the supporting surface. The two binding modes of the different functional groups differ with respect to the orientation of the ligand termination. The carbonitrile moiety points directly towards the metal center, whereas the hydroxy ligands are directed slightly off center, which accounts for the chirality of the binding motif in the latter case. These features are intrinsic properties of the ligand system and have to be taken into account when designing coordination architectures. The results demonstrate that surface-assisted assembly can lead to unusual coordination motifs that are generally not found in conventional 3D bulk phases. This effect is attributed to the presence of the surface, where hybridization of the metal orbitals with the metal states of the substrate causes unusual redox states (see Sect. 3.3). In addition, the preferred flat bonding of the aromatic system favors such unusual binding modes.

In a systematic study, the engineering of a series of honeycomb networks assembled from a series of the ditopic dicarbonitrile molecular bricks and Co atoms on Ag(111) was reported [124]. This approach enabled fabrica-

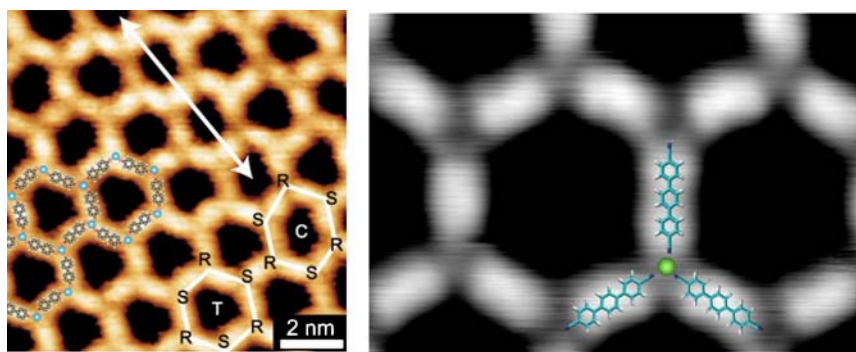


Fig. 7 Surface coordination motifs with threefold symmetry. *Left*: STM topograph displaying the hexagonal Fe-biphenolate network assembled on Ag(111). Different cavity types are highlighted in *white frames* and the handedness of the coordination centers are indicated by *S* and *R*. *Right*: high-resolution image of the Co-NC-Ph₃-CN honeycomb network assembled on Ag(111). Tentative models are superimposed over the data. Adapted from [122, 124]

tion of size- and shape-controlled open nanomeshes with pore dimensions up to 5.7 nm. For the investigations, linear dicyanitrile-polyphenyl molecular linkers (abbreviated NC-Ph_{*n*}-CN, whereby *n* can be 3, 4, or 5) were synthesized [100], motivated by the fact that carbonitrile compounds are known to coordinate strongly to transition metal centers [212, 213]. All ditopic molecular bricks have the same functional endgroups, while their lengths increase with *n* from 1.66 via 2.09 up to 2.53 nm. Indeed, the STM data reproduced in Figs. 7 and 8 demonstrate that by the controlled reaction of cobalt centers with preadsorbed linker molecules, a series of open nanomeshes with a tunable cavity size can be realized. The area of the enclosed hexagons increases stepwise with the number of phenyl rings incorporated into the molecular linker's backbone. Accordingly, the cell size expands stepwise from ≈ 10 via 15 up to 20 nm² for *n* = 3, 4, 5, respectively. While the 20 nm² nanopores achieved with NC-Ph₅-CN linkers represented a record for the most open surface-confined nanomesh realized by self-assembly, in more recent studies the limits were extended even further with a NC-Ph₆-CN linker [214].

It is known from the well-documented inorganic epitaxy studies that substrates play a crucial role in determining the adlayer structures. Related rules have been established for organic layers [215]. Parameters like the atomic lattice constant, crystalline orientation, and atomic steps have to be taken into

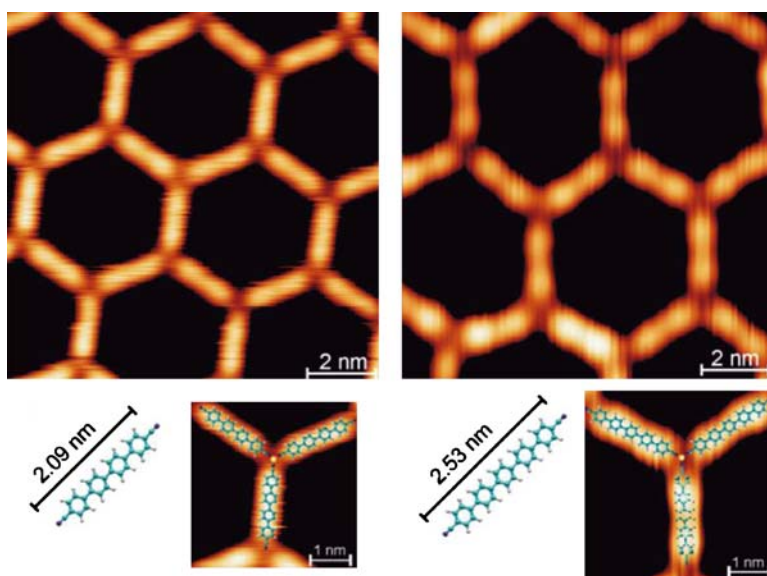


Fig. 8 Tunable metal-organic honeycomb nanomeshes with designed dicyanitrile linear linkers. *Upper panel:* STM images show the result of Co-directed assembly of NC-Ph₄-CN, and NC-Ph₅-CN. *Lower panel:* molecular structure and length along with models of the threefold Co-carbonitrile coordination motif. Adapted from [124]

account. For the metal-directed organization, the substrate influence is also of importance and needs to be assessed. Detailed investigation of the structural parameters of TPA, BDA, and TDA networks reveals the templating effects of the underlying substrate [207]. Besides the common feature of diiron coordination centers in fully reticulated network domains, the structures of the three molecules differ markedly in the coordination configuration and network geometries. These differences are attributed to the adsorbate–substrate coupling that plays a decisive role in the determination of the local coordination geometry. For instance, the Fe–Fe spacing in the BDA structure amounts to only 3.7 Å, thus being considerably smaller than in the TPA networks. In addition, the coordination configuration of BDA and TDA is different from the distorted square-planar geometry found for the Fe–TPA structure. Although the exact configuration cannot be deduced from the STM images, the spatial attachment of the ligands suggests either a planar trigonal geometry or a distorted tetrahedral coordination, whereby the former has been indeed observed for hydroxy functional moieties on the same surface. Besides the local coordination geometry, the network orientation with respect to the substrate lattice is different for the three molecules. In particular, the BDA and TDA molecules align along the [010] and [001] directions, whereas the TDA network orientation deviates slightly from the high symmetry [010] and [001] directions, implying that the structure is not precisely commensurate to the surface lattice. The influence of the substrate also has consequences for the shape of the cavities, whose size reflects the length of the linkers. It is proposed that the network structures are dominated by three different factors, the molecular adsorption energy, the Fe adsorption energy, and the Fe–carboxylate binding energy. The competition between the most favored molecular and metal adsorption sites and optimal coordination bonds determines the final topology. Thus the change of the molecule backbone strongly affects the geometries.

This mechanism is expressed explicitly when a symmetry mismatch between networks and substrate atomic lattices is present [122]. On the (100) facet the hexagonal Fe–hydroxyl networks are strongly distorted, resulting in a complicated arrangement of different cavity types but preserving the honeycomb topology. This ultimately limits the domain size. In contrast to the (100) surface, the networks grow continuously over entire terraces of the Ag(111) surface. The formation of highly symmetric hexagons is a consequence of the matching symmetry of the underlying substrate. Moreover, the achiral coordination nodes of the dicarbonitrile networks facilitate the growth of extended domains. The observed templating effects are a consequence of the preferred adsorption sites of the molecules and metal adatoms. Especially on the (100) surface, the network nodes of the honeycomb structure cannot adsorb on identical sites and therefore slight displacements are caused and the network is deformed. Nevertheless the metal–ligand bonding dictates the symmetry of the coordination motif.

In the case of rectangular Fe-TPA- or Co-TPA-coordination grids grown on the threefold Au(111) quasihexagonal substrate [121], the mismatch of the symmetries is merely reflected in limited domain sizes, which is significantly smaller than that of pure organic layers on the same substrate [216]. In conjunction with model calculations (see discussion below), the formation of the network is a result of the intrinsic properties of the binding mode between the transition metal ions and the carboxylate linkers. This linkage can overcome the templating influence of the rather low corrugated Au(111) surface. The driving forces for metal-terephthalate formation on Au(111) are determined primarily by the strength of the metal-carboxylate bond. Similar behavior was encountered in Mn-coordinated carboxylate lattices on the same surface [208], although much larger domains could be obtained.

To date, the networks based on dicyanitrile coordination of Co centers on the smooth Ag(111) substrate are of the highest structural quality. The honeycomb nanomeshes are thermally robust while extending over μm^2 large areas as single domains. Their high degree of regularity is visualized by the large scale STM topography in Fig. 9b. Histograms of the size distribution of the hexagonal cell underline the nearly perfect geometric order within the metal-organic networks (cf. [124]).

In sharp contrast, the twofold pyridine-Cu-pyridine coordination is not strong enough to overcome the adsorbate-substrate interaction. It was shown that by adjusting the chain structure commensurability with the substrate, the stability and structure of the chains is strongly affected, i.e., the epitaxial fit of the molecular structure with the substrate lattice has profound effects on the assembly and stability of the structures. The discussion of the commensurability of the structures in [204] as well as the dynamics of the chain formation highlights once again the importance of the adsorbate-substrate interaction and their implications for the construction of such low-dimensional architectures.

There is yet another approach to surface patterning, which involves the spatial confinement of reactions on surfaces, e.g., by controlling the formation of clusters or assembly of metal-organic complexes on a restricted area on the substrate. For instance, the dislocation pattern provided by the reconstructed Au(111) surface [217] provides a means to create transition-metal island arrays via self-organized growth of Fe or Co [120]. By tuning the local-reaction conditions with codeposited terephthalate linker molecules, one can follow coordination reactions [120, 121, 218, 219] and synthesize distinct low-dimensional metallosupramolecular systems, including regularly spaced Fe-terephthalate ribbons. With a careful exploitation of kinetic limitations, the corresponding gratings reflect the substrate chevron pattern, with their extension only limited by the terrace morphology rendering a mesoscopically ordered template structure [120].

One of the first intentions to test the usability of the described nanoporous superlattices was the study of inclusion of guest molecules into the open cavi-

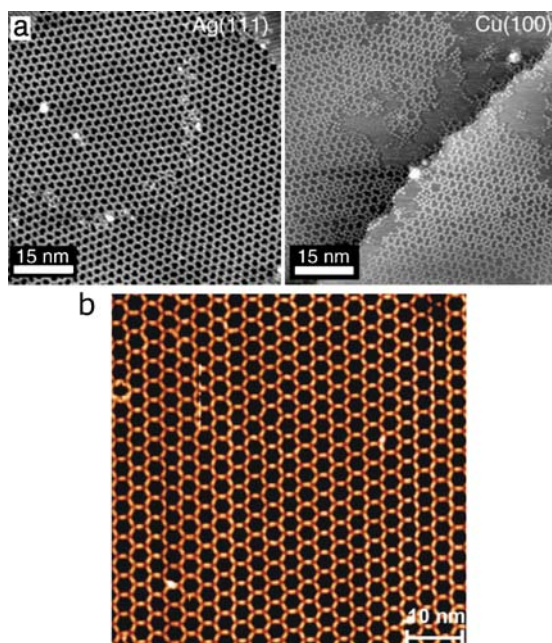


Fig. 9 Mesoscopic order of metallosupramolecular networks. **a** STM overview images showing the Fe-biphenolate networks assembled on Ag(111) (*left image*) and Cu(100) (*right image*). Two large domains on the Ag(111) surface are separated by a domain boundary. Three different domains are discernible on the Cu(100) surface. The size of the domains is considerably smaller on Cu(100) than on Ag(111). **b** The high lattice regularity extending in μm domains of Co-dicarbonitrile networks is shown by the large-scale STM image for the NC-Ph₃-CN linker. Adapted from [122, 124]

ties of the arrays revealing the underlying substrate. The appreciable thermal stability and overall robustness of the metal-organic networks makes them ideal templates for the (selective) adsorption of guest molecules and their templating on the surface. The cavities of the polybenzene carboxylate networks, as reported above, can be controlled by the backbone length of the linker molecules. The surrounding cavity consists of rather inert phenyl rings, weakly interacting with other functional groups. The size of the cavities was used to steer the interaction of C₆₀ molecules with the copper substrate and also the number of interacting C₆₀ molecules per pore (Fig. 10a,b) [115]. Furthermore, it was shown that besides the effect on the adsorbate-substrate interactions of the different pore sizes, the functionalization of the cavity rim by replacing the rod-like TPA molecule with TMLA (featuring an additional carboxylate side group available for interactions with guest species) can significantly alter the effective interaction of the C₆₀ with the pores and substrate. Recently open Mn-based carboxylate networks were also used to capture C₆₀ dimers [220].

The cavities of the FeTMA arrays presented above, emerging from the hierarchical self-assembly of TMA molecules in the presence of Fe adatoms, feature identically shaped hosts of about 1 nm, equally spaced by 3.43 nm and functionalized by eight carboxylate groups. It was successfully demonstrated that this network is capable of selective and reversible adsorption of a series of guest species, including C_{60} and small biomolecules (Fig. 10c) [221].

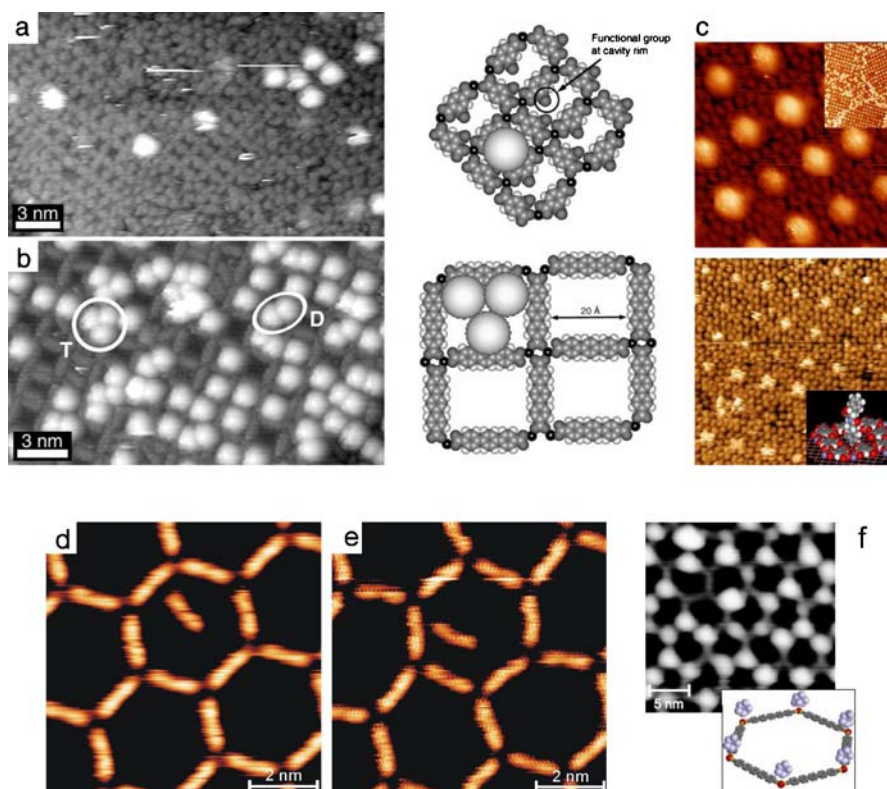


Fig. 10 Host-guest interactions and selective decoration at nanoporous coordination networks. **a, b** STM data and models showing the accommodation of C_{60} in nanoporous FeTMLA (**a**) and FeTDA (**b**) networks. Similar to the FeTPA grids, FeTMLA networks exclusively host C_{60} monomers. The indicated functional side-group strongly affects the chemical reactivity of the cavity. The mesoscale cavities in FeTDA networks can host C_{60} monomers, dimers (*D*) and trimers (*T*). **c** Binding of C_{60} (*upper image*) and diphenylalanine (*lower image*) in FeTMA nanocavities. The apparent fuzzy protrusions of the Phe-Phe is associated with molecular conformational changes during the STM imaging process. **d, e** Host cavities, formed by the metal-organic network of NC- Ph_3 -CN linkers and CO_2 where a single dicarbonitrile guest molecule is trapped. The confined species can be switched between two configurations by the STM tip. **f** Preferential decoration of network nodes by Fe clusters following exposure of the same nanomesh to a beam of Fe atoms at $T \sim 200$ K; the *inset* shows a schematic model. Adapted from [115, 124, 214, 221]

Metal–organic open networks similarly represent templates for the study of molecular motion processes in confined environments, as illustrated with the confined guest species in the dicyanitrile-based nanomeshes depicted in Fig. 10d,e. Individual dicyanitrile linkers confined in the cavities formed by $[(\text{NC-Ph}_3\text{-CN})_{3/2}\text{Co}]_n$ nanomeshes, can be, for instance, rotated back and forth between two metastable positions. On the other hand, the honeycomb nanomeshes qualify as templates to steer the formation of Fe and Co nanostructures by offering nucleation sites at their rims and nodes. They notably can be used to control the surface distribution of Fe clusters that comprise a small number of atoms. The preferential nucleation sites are the ligands of the networks for temperatures in the range 90–120 K and the networks nodes for temperatures in the range 190–220 K (cf. Fig. 10f) [214].

3.3

Computational Modeling

The theoretical analysis of metal–organic complexes in contact with solid metal substrates has been addressed by ab initio calculations based on density functional theory (DFT). The reported results of the Fe- and Co-terephthalate dinuclear grids [121,222], the Fe–TMA chains [203], and isolated adsorbed porphyrins on noble metal surfaces [127,165,223] reveal the interplay of the involved interactions between ligands and metal ions as well as adsorbates and substrate in the determination of the electronic and magnetic properties of the metal centers. For the $3d$ metal-carboxylate systems presented above the molecules are rather flat on the surfaces with their carboxylate groups bending towards the surface, such that oxygen atoms reside on top of the Cu surface. This signifies the strong interaction of the carboxylate groups with the substrate, which has been suggested by earlier findings and accounts for the strong templating effects.

Besides the elucidation of the adsorbate structure of the metal–TMA chains, DFT calculations give also insight into the electronic structure of the coordination centers, in particular the spin states [203]. It was found that the projected density of states displays an appreciable splitting between the majority and minority spin electronic d states. Moreover, the spin polarization of $3.3 \mu_B$ is comparable to the polarization of an isolated Fe adatom ($3.2 \mu_B$). Consequently the coordination to the carboxylate groups does not affect the electron localization at the coordination center, i.e., does not quench the spin magnetic moment.

For the diiron FeTPA system, DFT charge density calculations reproduce the main features appearing in the STM data (see Fig. 11a) and provide an atomistic description of the respective electronic and geometric structure [222]. The corresponding model in Fig. 11a shows a close-up view of the carboxylate-bridged diiron center. DFT indicates Fe–O bond lengths of

2.01 Å (equatorial) and 2.24 Å (axial), respectively, close to values in 3D Fe-carboxylates [54].

A further striking consequence of the strong lateral Fe-carboxylate coupling is the modified Fe-substrate bonding distance upon embedding of the Fe centers in the metal-organic array. Compared with isolated Fe adatoms in a fourfold hollow position, those in the Fe-TPA grid are vertically lifted by 0.6 Å, and in addition the Fe atoms are laterally displaced from the high-symmetry substrate positions (Fe-Fe spacing of 4.4 Å). Comparative calculations for the freestanding isostructural 2D Fe-TPA layer signal that the unsupported metal-organic array's properties are close to those of the adsorbed grid; i.e., the Cu(100) square atomic lattice represents an excellent template. The strong hybridization between the Fe and Cu states prevents a conclusive analysis of the Fe oxidation state. Nevertheless, there also is a marked splitting between the spin majority and minority states in this system, as observed in the projected density of states presented in Fig. 11b. The resulting spin polarization accounts for strongly magnetized Fe centers bearing a magnetic moment of $3.4 \mu_B$, coming close to the spin moment

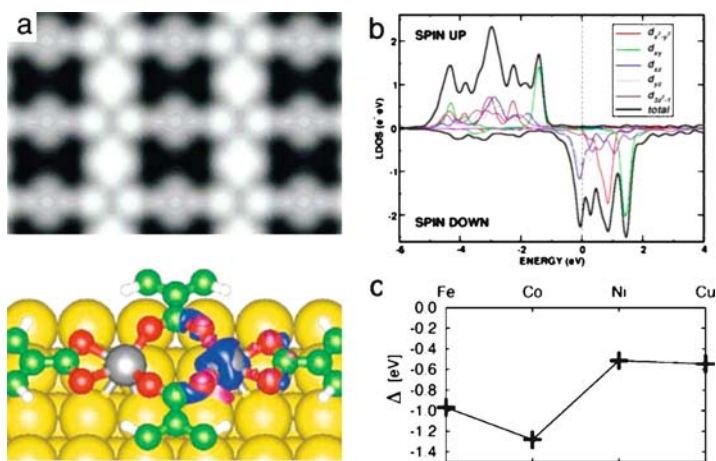


Fig. 11 Modeling of Fe-carboxylate dinuclear bond motif by ab initio methods. **a** STM image simulation showing contours of constant local density of states (LDOS) at the sample Fermi level derived from the DFT modeled Fe-diterephthalate grids on Cu(100). The graph below shows a perspective view of the diiron unit. The substrate square atomic lattice is represented by large spheres, the linkers and the Fe centers of the grid by spheres with rods symbolizing the chemical bonding. Fe charge rearrangement contour levels are indicated for the center at the right, drawn with respect to a removed iron atom, at $\pm = 0.004 e^-/\text{\AA}^3$, whereby the intensity indicates increased (dark) and decreased (light) electron density, respectively. **b** Spin-polarization of Fe centers as evidenced in the projected density of electronic states on the Fe atomic d orbitals. **c** Driving force Δ for metal-carboxylate formation on Au(111) as a function of different transition-metal species. Adapted from [222] **a,b** and [121] **c**

in the mononuclear Fe trimesate chains grown on the Cu(110) substrate. Moreover, the DFT results reveal a magnetic coupling between the Fe centers in diiron units. This is in line with the previously observed magnetic coupling in 3D oxygen-bridged dinuclear iron complexes [224], but in the present case its nature (ferro- or antiferromagnetic) could not be conclusively determined.

The dependence of the metal–ligand formation on the nature of the coordination center was addressed by DFT calculations for the metal–TPA system on Au(111) [121]. The energetics of the process involve the chemisorption energy of the adsorbed metal–TPA complex, the individual adsorbates, i.e., metal adatom and molecule, and the gas phase molecules/products. It was assumed that the major contribution is given by the metal–surface and metal–carboxylate interaction, whereas the molecule–surface interaction does not vary strongly with different metals bound to the molecule. The interaction energy is further divided into the binding energy in the gas phase, the adhesion energy of the metal adatom on the surface and the cohesion energy of the bulk metal, i.e., the energy gain of a gas phase atom incorporated into an island. It was found in the study of four metal centers (Fe, Co, Ni, and Cu) that the strongest binding energy in the gas phase exists for Co, followed by Fe and, by some distance, the less reactive Ni and Cu atoms. The transition metals generally have a strong tendency to form clusters and islands, so the binding energy to the carboxylate group determines the driving force for the complexation of the metals. The relatively low cohesive energy of Cu compared to the other metals makes it easily available on the surface for metal–ligand bonding, although the binding energy to the carboxylate groups is rather low (Fig. 11c).

The theoretical treatment of the interesting class of macrocyclic four-dentate ligands like porphyrins and phthalocyanines has also been performed with DFT calculations. On metal surfaces in the submonolayer regime the molecules are found to chemisorb parallel to the surface, in accordance with STM observations, with rather weak binding energies on Au or Ag substrates [125, 127, 165, 223]. The identification of binding sites, especially for the metal center, and the charge transfer between molecule and surface provide information in great detail about the spin-state and magnetic properties of the adsorbates. The deformation and conformational changes of the molecules upon adsorption affects the hybridization of the metal *d*-states with the surface and has consequences for the spin-polarization of the coordination centers [126, 223, 225].

Also, the threefold coordination of the Co centers in the dicarbonitrile nanomeshes described above could be rationalized with the help of DFT calculations. For the modeling, the molecular linkers were simplified as NC–Ph₁–CN retaining the carbonitrile endgroups that interact with the Co centers. In addition, the molecules were confined in a plane in accordance with the STM data, showing that the aromatic polyphenylene linkers are ad-

sorbed in a flat configuration with the molecular axis parallel to the metal substrate [124]. To assess the interaction of the Co center with the underlying surface, calculations were performed of both free planar compounds and complexes where a cluster of four Ag atoms was placed underneath the coordinated Co atom (cf. Fig. 12). A comparison between threefold and fourfold coordination without and with an Ag cluster placed below the coordination node shows that including an Ag cluster leads to a preferred threefold coordination (Fig. 12). Consideration of the binding energies within the node indicates that the interaction of the cobalt atoms with the surface is a key factor in favoring a 2D network with a threefold coordination of the organic

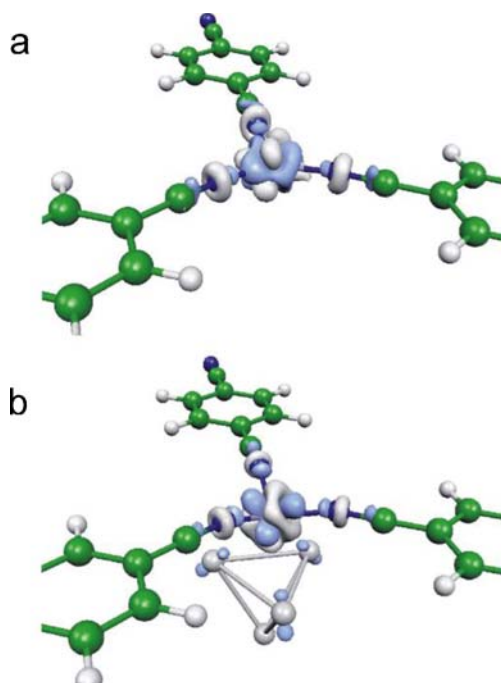


Fig. 12 DFT calculations addressing the threefold coordinated Co centers in the honeycomb nanomeshes obtained with dicarbonitrile linkers on Ag(111). **a,b** Plots of the induced charge density around the cobalt atom in threefold coordination of a model compound (NC-Ph₁-CN) without (**a**) and with (**b**) the presence of an Ag₄ cluster underneath the transition metal center. The image displays the electron density redistribution around the Co atom due to the bond formation with the ligands. *Dark shading* means charge depletion, and *light shading* charge accumulation ($0.01 e/\text{\AA}^3$). Without an Ag cluster the binding energy within the node for fourfold coordination exceeds threefold by 460 meV (energy per ligand: 1.82 eV threefold and 1.48 eV fourfold). With an Ag cluster placed below the coordination node threefold exceeds fourfold by 70 meV (energy per ligand: 1.65 eV threefold and 1.22 eV fourfold). Adapted from [124]

ligands. Accordingly an appreciable electronic hybridization between the Co and Ag atoms occurs, as visualized in Fig. 12.

4

Metal Ion–Ligand Assemblies at the Solid–Liquid Interface

Initial work on coordination-controlled self-assembly at interfaces was inspired from the field of self-assembled monolayers (SAMs) [226, 227]. This means the fabrication of an organized molecular layer, where the reactive group at one end of the molecule (e.g., a carboxylate, reactive silane, or thiol) is anchored to the surface, and non-covalent intermolecular interactions mediate an in-plane ordering. The functional group at the other end of the molecule can be chosen to be an appropriate ligand (e.g., hydroxamate, phosphonate, carboxylate) for the coordination of metal ions provided by a solution or an atomic beam. Thus coordination-controlled multilayers can be engineered by sequential adsorption (cf. [62, 228–230] and references therein). The control of such systems is also of interest for electronic nanoscale devices [230–233]. On Au-supported self-assembled monolayers, coordination cages based on cavitands complexed with pyridine-coordinated Pd ions were realized [234]. More recently, the SAM-template approach was refined to direct the growth of metal–organic frameworks [235, 236]. These findings bear promise for the interfacing of 2D to 3D systems [237] and the development of novel functional materials based on 3D metal–organic framework or metallocupramolecular synthesis protocols.

An early report involving metal complexes on surfaces deals with the in-situ coordination reaction of deposited 2,2'-bipyridine ligands with Pd(OAc)₂ at the phenyloctane graphite interface, which results in a complete reorganization of the organic monolayer [112, 117], whereby the coordination reaction presumably takes place in the concomitant solvent volume after detaching the 2,2'-bipyridine ligands from the surface and redeposition of the formed 2,2'-bipyridine ligands–palladium acetate complexes [96]. Pyridine ligands were similarly employed for a bimodal self-assembly procedure for the organization of either cavitand dimers or oligomers on graphite [238]. A related protocol was used to coordinate 4-pyridyl-substituted terpyridyl ligands with Co(II) and Pd(II) metal ions, leading in both cases to strictly 1D structures on graphite [239], whereas the same ligand preassembled with Ru(II) and Os(II) metal ions and drop-casted on Pt(100) leads to molecular arrays exhibiting relatively low internal order but a high degree of internal freedom and mobility [240]. Also the metal-directed assembly of terpyridine-containing dendrimers could be achieved in an interfacial reaction [241]. A more sophisticated synthetic design based on the terpyridine motif features two enantiomerically pure bridging ligands giving controlled access to domains of highly ordered chiral coordination polymers. Thereby, each enan-

tiomorphic ligand is mixed with Fe(II) metal ions in CH₂Cl₂/water mixture and deposited on an HPOG substrate yielding domains of interfacially stabilized helical coordination polymers of opposite sense of rotation, detectable directly by STM imaging [108, 242].

Being another classical ligand system, a series of salophen complexes [salophen = *N,N'*-(*o*-phenylene)bis(salicylideneimine)] of Cu(II), Ni(II), and Co(II) metal ions was prepared and their 2D assemblies investigated at the liquid–solid interface by STM. Depending on the chain lengths of the alkyl substituents, two different adlayer organizations, parallelogram and honeycomb, were observed [243]. However, only isolated mononuclear complexes are formed by the distinctive metal ion–ligand interactions, while the intermolecular complex-to-complex interaction is mediated by van der Waals interactions and hydrogen bonds. A recent study reported an even more intricate 2D assembly scheme for surface-supported metal–organic clusters: a single nanoporous coordination structure, in which a fractal polymeric macromolecule (recognized as Sierpinski gasket) is composed of bis-terpyridine tectons coordinating 36 Ru and six Fe atoms [244].

The formation of highly-ordered 2D monolayers from preassembled [$n \times n$] metal ion arrays on surfaces represents a two-tiered self-assembly process (see Scheme 2, left): (i) The [$n \times n$] metal ion arrays are formed in a bulk self-assembly step in solution from their constituents (organic ligands and metal ions). (ii) Subsequently, the [$n \times n$] metal ion arrays are self-assembled themselves to densely packed domains of monolayers on the graphite surface [118]. The first self-assembly process relies on the read-out of the coordination instructions stored in the ligands and the metal ions, while the second is steered by van der Waals forces between the metal ion arrays on the one side and between arrays and graphite surface on the other side. Due to the flat, square-like geometry of the [$n \times n$] metal ion arrays, this second self-assembly process automatically results in a highly-ordered “grid-of-grids” superstructure under 2D confinement. Thus, monolayers of [$n \times n$] metal ion arrays exhibit a twofold supramolecular matrix-structure: (i) internally by the ligand-directed coordinative positioning of the metal ions and (ii) externally by the van-der-Waals directed formation of the “grid-of-grids” superstructure. Single metal ion addressing the inside of isolated metal ion arrays could be achieved electronically by use of scanning tunneling spectroscopy technique called current-induced tunneling spectroscopy (CITS) [150].

Different supramolecular bi- and tetranuclear Pd(II) and Pt(II) complexes of square- or rhomb-like shape were deposited under potential control from aqueous electrolyte on a Cu(100) electrode surface, which was precovered by tetragonal pattern of chloride anions (Fig. 13) [116, 151, 245]. Although, partial decomposition was observed, it could be concluded that contact with the surface does not affect the metal coordination algorithms, but actively steers the adsorption parameters (relative orientation, internal conformations, etc.)

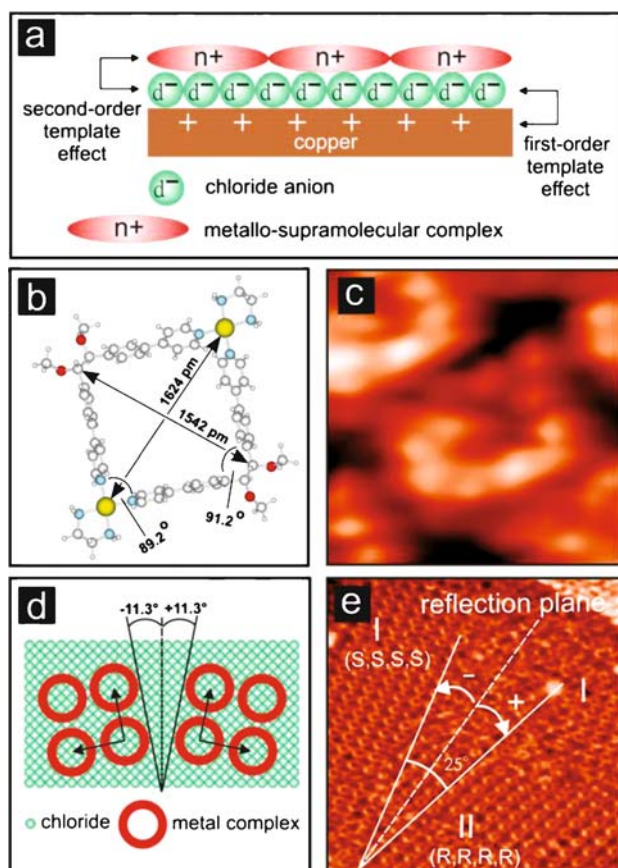


Fig. 13 Binuclear Pt_2^{II} -square complexes on surfaces. **a** Scheme showing the different tiers of template steering the self-assembly of the supramolecular $\text{Pt}_2^{\text{II}}(\text{L})_2$ complex on a $\text{Cu}(100)/\text{Cl}^-$ -substrate. **b** Molecular structure and dimensions of a $[\text{Pt}_2^{\text{II}}(\text{L})_2]^{4+}$ cation. For comparison, **c** STM data showing a single complex. **d** Schematic and **e** experimental representation of the segregation of a racemic mixture of $[\text{Pt}_2^{\text{II}}(\text{L})_2]^{4+}$ molecules exhibiting surface-confined resolution into 2D enantiopure domains. Adapted from [245]

of the supramolecules on the metallic surface. The introduction of chirality into the ligand systems induces the formation of single domain orientation, or, if racemic mixtures are used, segregation into enantiomerically pure surface-confined domains (Fig. 13d,e). By a similar approach, the organization of previously self-assembled supramolecular metallacyclic $\text{Pt}(\text{II})_4$ rectangles was investigated on graphite and $\text{Au}(111)$ surfaces. The rectangles adsorb on both substrates in a different way: On graphite, they stand on the long edge, while on $\text{Au}(111)$ they lay flat on the surface forming linear chains [152, 246]. More recently, their ordering in monodisperse islands could be achieved with the help of a molecular template providing an array

of nanocavities [247]. Additionally, trimeric Zn(II) complexes of polypyrrol imine ligands with distinct triangular shape were studied on a Au(111) surface [248].

Monolayers of tetranuclear $[2 \times 2]$ Co_4^{II} metal ion arrays were generated by drop-casting the supramolecules on an atomically flat graphite surface (HOPG). The highly ordered supramolecular surface structures consisting of densely-packed flat-lying $[2 \times 2]$ Co_4^{II} metal ion arrays (MIAs) of rectangular shape are formed spontaneously from dilute acetone solution as almost defect-free domains of up to $0.5 \mu\text{m}^2$ (Fig. 14). The domain formation proceeds outwards from single nucleation points, a process which might be considered 2D crystallization.

Certain substitution patterns at the organic ligands also provoke “on-the-edge” orientation of the metal ion arrays with respect to the surface. But, most of the observed metal ion $[2 \times 2]$ arrays result in flat tiles forming a “grid-of-grids” superarray, in which the presence of the $[2 \times 2]$ metal ion grids is reflected by the $2.5 \times 2.4 \text{ nm}$ periodicity in agreement with the molecule size determined by X-ray crystallography [107, 249]. In a similar way, $[3 \times 3]$ Mn_9^{II} metal ion arrays were studied on both HOPG and Au(111) surfaces [250, 251].

By application of a voltage pulse through the STM-tip on the monolayer of metal ion arrays, a single $[2 \times 2]$ Co_4^{II} metal ion array could be lifted, leaving a square-like hole of the dimension of the molecule (see Fig. 14b). The migration rate of the hole was measured to be 200 times slower than in a monolayer of cycloalkanes, reflecting the degree of adsorption of the molecules to the

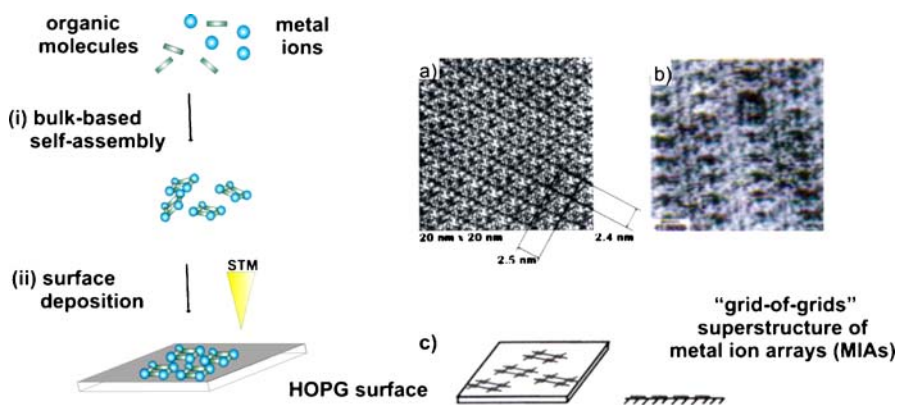


Fig. 14 Schematic representation of the deposition of metal ion arrays (MIAs) on surfaces. **a** STM-image of the monolayer of $[2 \times 2]$ Co_4^{II} metal ion arrays on graphite. The 2D periodicity of the “grid-of-grids” network is shown with $2.5 \times 2.4 \text{ nm}^2$. **b** A hole in the supramolecular monolayer is produced by potential induced lifting of a single $[2 \times 2]$ Co_4^{II} molecule with the STM-tip. **c** Schematic representation of the disposition of the MIAs at the surface (*top and side view*). Images adapted from [107]

graphite surface [107]. Further insight into the intramolecular electronic situation of isolated single $[2 \times 2]$ Co^{II} metal ion arrays at room temperature and ambient conditions was gained by CITS [119]. These experiments allowed, by selective mapping of the highest occupied molecular orbitals (HOMOs), the localization of the positions of the incorporated Co^{II} ions. First-principle DFT calculations confirmed that in these type of molecules the HOMOs possess a large d -character such that they are strongly localized around the positions of the metal ions. Consequently, the projection of the CITS maps at certain negative tunneling biases indicates electronically the cornerstone positions of the four Co^{II} metal ions (Fig. 15a,b) [118] (for a related discussion of the imaging of Cu-complexes on graphite see [252]). The same technique was successfully applied to visualize the metal ions in the higher homologous $[3 \times 3]$ Mn_9^{II} and $[4 \times 4]$ $\text{Mn}_{16}^{\text{II}}$ MIAs aligning nine and 16 manganese ions, respectively. The obtained CITS maps mirror the structural situation within the metal ion arrays since, although very regularly arranged, the metal ions in these higher homologues display a more lozenge-like structure (Fig. 15c). This structural deviation from the optimal square-like arrangement can be attributed to the “pinching-in” of the organic ligands during metal ion coordination, reflecting the importance and the consequences of sufficiently instructed metal-ligand interactions for the outcome the self-assembly processes [251].

Cage compounds were also studied at surfaces. In particular polyoxometallates (POMs), which are early-transition-metal oxygen clusters, give rise to a certain interest in view of their potential applications due to the very robust cage scaffold and broad variety in shape, size, and composition [253]. This class of compounds, often described as soluble metal-oxide fragments, receives increasing attention mostly due to its multitude of interesting catalytic, electronic, magnetic, medical, thermal, and optical properties [254]. Recently, the synthesis of an unprecedented Cu_{20} -containing polyoxotungstate of large

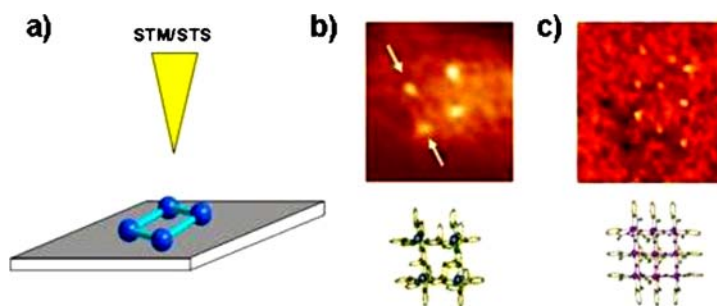


Fig. 15 **a** Schematic principle showing the metal ion array on a graphite surface; **b** and **c** show the results of the locally resolved current-induced tunneling spectroscopy (CITS) measurements of a $[2 \times 2]$ Co_4^{II} and $[3 \times 3]$ Mn_9^{II} indicating the position and arrangement of the respective metal ions. Adapted from [150]

size and high symmetry by self-assembly techniques was reported [255]. The wheel-shaped $[\text{Cu}_{20}\text{Cl}(\text{OH})_{24}(\text{H}_2\text{O})_{12}(\text{P}_8\text{W}_{48}\text{O}_{184})]^{25-}$ represents a transition metal-substituted derivative of $[\text{H}_7\text{P}_8\text{W}_{48}\text{O}_{184}]^{33-}$ and incorporates more Cu^{2+} ions than any other polyoxometalate known to date. The present Cu_{20} wheel can be considered an oxygen-copper cage sitting as a hub in the center of a large polyoxotungstate wheel. The Cu_{20} cluster is therefore effectively shielded from the environment but sufficiently open for investigations with the STM [256]. A second supramolecular cage compound, a self-assembled cuboctahedron comprising 12 Pd(II) metal ions and 24 organic ligands of pyridine type, was studied on a HOPG surface. The investigations have proven that this cage also maintains its integrity under near-surface conditions, despite the relative lability of the constituent Pd(II)-N bond [257]. More recently, the assembly of nanosize coordination cages on Si(100) was achieved using a two-step procedure [258].

1D coordination polymer assemblies have attracted much attention in the development of new functional materials owing to such properties as zeolitic behavior, conductivity, luminescence, magnetism, spin-crossover, and non-linear optical effects [76]. 1D coordination chains in solution were obtained from Fe and ditopic bis-terpyridines on graphite [109]. Also, polymeric rotaxane chains consisting of cyclodextrins-dipyridine units connected by coordination with Ni ions [259], and $[\text{CuBr}-(\text{isonicotinic acid})]_n$ polymeric chains [260] were investigated regarding their surface assembly behavior.

In related investigations, a series of structurally similar polymers containing different aromatic amino acid ligands were investigated in order to estimate the influence of the substituents on the local surface properties. Towards this end, the cationic coordination polymer $[[\text{Zn}(\text{L})]_n] (\text{CF}_3\text{SO}_3)_n$ (L = dipicolylglycyl tyrosine) was deposited on HOPG and investigated with regard to its local tunneling properties (Fig. 16) [261]. More recently, fibres of $[\text{Ru}_2\text{Br}(\mu\text{-O}_2\text{CET})_4]_n$ polymers have also been isolated on different surfaces [262].

Samples of $[[\text{Zn}(\text{L})]_n] (\text{CF}_3\text{SO}_3)_n$ on HOPG were prepared by allowing 10^{-9} M aqueous solutions of pH 5 to 6 to evaporate under air. It was shown by topographic STM investigations that the polymer adopts two different structures depending on the local environment of the substrate: (i) a double-helical plait is formed on undisturbed flat surface areas, and (ii) linearly stretched polymer strands are formed along the steps of the substrate (see Fig. 16b). Apparently, the structure change is a consequence of different strength polymer-substrate interactions between $[[\text{Zn}(\text{L})]_n] (\text{CF}_3\text{SO}_3)_n$ and the HOPG substrate.

Furthermore, a 1D ribbon-like coordination polymer could be obtained by the coordination of 2,5-dihydroxybenzohydroquinone (DHBQ) with Cu(II) ions in aqueous solution directly at the solid-liquid interface on an Au(111) substrate. The authors advocate a "surface-assisted self-organized" growth mechanism, which involves in-situ deprotonation and metal coordination

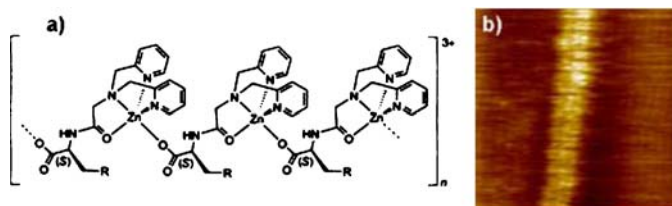


Fig. 16 The cationic coordination polymer $[[\text{Zn}(\text{L})]_n](\text{CF}_3\text{SO}_3)_n$: **a** representation of the molecular structure, $\text{R} = \text{Ph-OH}$; **b** topographic STM image on HOPG revealing the 1D character under near-surface conditions. Adapted from [261]

processes under the steering influence of the Au(111) surface. Since these processes seem to yield ordered monolayers of 1D $[\text{Cu-DHBQ-}]_n$ ribbons if the gold substrate is preheated, an activation barrier seems to be involved in the formation of the supramolecular structure; indeed an argument in favor of in-situ coordination processes under surface confinement [263].

5 Résumé and Perspectives

The presented double road map towards surface-confined metallocsupramolecular nanostructures constitutes part of the future toolkit needed to put into reality steered *aufbau* and controlled manipulation of functional interfaces or operational surfaces. The described findings reveal that both methodologies (i.e., direct surface-assisted complexation and deposition of pre-fabricated species) employ metal-directed assembly protocols to achieve unique coordination systems in environments of reduced dimensions. They are conceivable for a great variety of molecular systems and can be applied to substrates with different symmetries and with different physical and chemical nature. The intrinsic physicochemical properties of the metal centers (e.g., unsaturated coordination spheres, their redox, spin, magnetic, and electronic states) present a formidable playground for many exciting further developments, ranging from molecular electronics and magnetism to single-site heterogeneous catalysis. The templating of specific host-guest interactions foreshadows the use of nanoporous metal-organic coordination networks for both patterning purposes or investigations of surface chemical reactions in controlled surroundings. Furthermore, they may serve as scaffolds for the organization of separated, regularly distributed magnetic nanoclusters and bear the potential to confine complex synthetic or biological guest molecules in tuneable spaces where their motion or switching can be regulated.

Acknowledgements The work reviewed here has been partially supported through several funding schemes, as mentioned in the original papers. It would not have been possible

without the dedication and talent of the involved students, researchers, and cooperating scientists to whom the authors are very thankful.

References

1. Werner A (1893) *Z Anorg Chem* 3:267
2. Werner A (1912) *Annu Chem* 386:1
3. Wyckoff RWG, Posnjak E (1921) *J Am Chem Soc* 43:2292
4. Dickinson RG (1921) *J Am Chem Soc* 44:2404
5. Bethe H (1929) *Ann Phys* 395:133
6. Bethe H (1930) *Z Phys* 60:218
7. Bersuker IB (1996) *Electronic structure and properties of transition metal compounds: introduction to the theory*. Wiley, New York
8. Becquerel J (1929) *Z Phys* 58:205
9. Van Vleck JH (1932) *J Chem Phys* 3:807
10. Cotton FA, Wilkinson G (1988) *Comprehensive inorganic chemistry*. Wiley, New York
11. Wilkinson G, Gillard RD, McCleverty JA (1989) *Comprehensive coordination chemistry*. Pergamon, Oxford
12. Langmuir I (1916) *J Am Chem Soc* 38:2221
13. Taylor HS (1925) *Proc R Soc London A* 108:105
14. Volmer M, Adhikari G (1925) *Z Phys* 35:170
15. Becker JA (1926) *Phys Rev* 28:341
16. Cassel H (1926) *Naturwissenschaften* 14:103
17. Moll F (1928) *Z Phys Chem* 136:183
18. Schottky W (1928) *Z Phys* 14:63
19. Langmuir I (1932) *J Am Chem Soc* 16:2798
20. Langmuir I, Taylor JB (1932) *Phys Rev* 40:463
21. Lennard-Jones JE (1932) *Trans Faraday Soc* 28:333
22. Rideal EK (1932) *Trans Faraday Soc* 28:139
23. Volmer M (1932) *Trans Faraday Soc* 28:359
24. Becker JA (1933) *Trans Faraday Soc* 28:148
25. Langmuir I (1933) *Chem Rev* 13:147
26. Taylor JB, Langmuir I (1933) *Phys Rev* 44:423
27. Becker JA (1929) *Trans Am Electrochem Soc* 55:153
28. Davisson C, Germer LH (1927) *Phys Rev* 30:705
29. Lander JJ, Morrison J, Unterwald F (1962) *Rev Sci Instrum* 33:782
30. Ertl G, Küppers J (1985) *Low energy electrons and surface chemistry*. VCH, Weinheim
31. Duke CB (ed) (1994) *Surface science: the first thirty years*. *Surf Sci* 299/300:1–1039
32. Ertl G (1990) *Angew Chem Int Ed* 29:1219
33. Somorjai GA (1996) *Chem Rev* 96:1223
34. Ugo R (1975) *Catal Rev Sci Eng* 11:225
35. Plummer EW, Salaneck WR, Miller JS (1978) *Phys Rev B* 18:1673
36. Johnson KH, Balasz AC, Kolari HJ (1978) *Surf Sci* 72:733
37. Muetterties EL, Rhodin TN, Band E, Brucker CF, Pretzer WR (1979) *Chem Rev* 79:91
38. Nitschké F, Ertl G, Küppers J (1981) *J Chem Phys* 74:5911
39. Gavin RM, Reutt J, Muetterties EL (1981) *Proc Natl Acad Sci USA* 78:3981
40. Soriaga MP (1990) *Chem Rev* 90:771

41. Gibson DH (1999) *Coord Chem Rev* 185-186:335
42. Burwell RL Jr, Haller GL, Taylor KC, Read JF (1969) *Adv Catal* 20:1
43. Ferrari AM, Huber S, Knözinger H, Neyman KM, Rösch N (1998) *J Phys Chem B* 102:4548
44. Freund HJ (1997) *Angew Chem Int Ed* 36:452
45. Over H, Kim YD, Seitsonen AP, Wendt S, Lundgren E, Schmid M, Varga P, Morgante A, Ertl G (2000) *Science* 287:1474
46. Gong X-Q, Raval R, Hu P (2004) *Phys Rev Lett* 93:106104
47. Wang J, Fan CY, Sun Q, Reuter K, Jacobi K, Scheffler M, Ertl G (2004) *Angew Chem Int Ed* 42:2151
48. Copéret C, Chabanas M, Saint-Arroman RP, Basset J-M (2003) *Angew Chem Int Ed* 42:156
49. Thomas JM, Raja R, Lewis DW (2005) *Angew Chem Int Ed* 44:6456
50. Nozaki C, Lugmair CG, Bell AT, Tilley TD (2002) *J Am Chem Soc* 124:13194
51. Avenier P, Taoufik M, Lesage A, Solans-Monfort X, Baudouin A, de Mallmann A, Veyre L, Basset J-M, Eisenstein O, Emsley L, Quadrelli EA (2007) *Science* 317:1056
52. Tada M, Coquet R, Yoshida J, Kinoshita M, Iwasawa Y (2007) *Angew Chem Int Ed* 46:7220
53. Holm RH, Kennepohl P, Solomon EI (1996) *Chem Rev* 96:2239
54. Merckx M, Kopp DA, Sazinsky MH, Blazyk JL, Müller J, Lippard SJ (2001) *Angew Chem Int Ed* 40:2783
55. Groves JT (2003) *Proc Natl Acad Sci USA* 100:3569
56. Woggon W-D (2005) *Acc Chem Res* 38:127
57. Chen K, Mirkin CA, Lo R-K, Zhao J, McDevitt JT (1995) *J Am Chem Soc* 117:6374
58. Thorpe JM, Beddoes RL, Collison D, Garner CD, Helliwell M, Holmes JM, Tasker PA (1999) *Angew Chem Int Ed* 38:1119
59. Vestal CR, Zhang ZJ (2003) *J Am Chem Soc* 125:9828
60. Maeda Y, Okumura M, Daté M, Tsubota S, Haruta M (2002) *Surf Sci* 514:267
61. Aurora A, Cattaruzza F, Coluzza C, Della Volpe C, Di Santo G, Flamini A, Mangano C, Morpurgo S, Pallavicini P, Zanoni R (2007) *Chem Eur J* 13:1240
62. Condorelli GG, Motta A, Bedoya C, Di Mauro A, Pellegrino G, Smecca E (2007) *Inorg Chim Acta* 360:170
63. Hagfeldt A, Grätzel M (2000) *Acc Chem Res* 33:269
64. Lehn J-M (1995) *Supramolecular chemistry, concepts and perspectives*. VCH, Weinheim
65. Lehn JM (2002) *Proc Natl Acad Sci USA* 99:4763
66. Atwood JL, Davies JED, MacNicol DD, Vögtle F, Lehn J-M (1996) *Comprehensive supramolecular chemistry*. Pergamon, New York
67. Lawrence DS, Jiang T, Levett M (1995) *Chem Rev* 95:2229
68. Philp D, Stoddart JF (1996) *Angew Chem Int Ed* 35:1154
69. Swiegers GF, Malefetse TJ (2000) *Chem Rev* 100:3483
70. Fujita M, Umemoto K, Yoshizawa M, Fujita N, Kusukawa T, Biradha K (2001) *Chem Commun*, p 509
71. Leininger S, Olenyuk B, Stang PJ (2000) *Chem Rev* 100:853
72. Holiday BJ, Mirkin CA (2002) *Angew Chem Int Ed* 40:2022
73. Cheetham AK, Férey G, Loiseau T (1999) *Angew Chem Int Ed* 38:3268
74. Moulton B, Zaworotko MJ (2001) *Chem Rev* 101:1629
75. Férey G (2001) *Chem Mater* 13:3084
76. Janiak C (2003) *Dalton Trans*, p 2781
77. MasPOCH D, Ruiz-Molina D, Veciana J (2004) *J Mater Chem* 14:2173

78. Maspoch D, Ruiz-Molina D, Wurst K, Domingo N, Cavallini M, Biscarini F, Tejada J, Rovira C, Veciana J (2003) *Nat Mater* 2:190
79. Yaghi OM, O'Keefe M, Ockwig NW, Chae HK, Eddaoudi M, Kim J (2003) *Nature* 423:705
80. Kitagawa S, Kitaura R, Noro S (2004) *Angew Chem Int Ed* 43:2334
81. Hosseini MW (2005) *Acc Chem Res* 38:313
82. Gianneschi NC, Masar MS, Mirkin CA (2005) *Acc Chem Res* 38:825
83. Badjic JD, Nelson A, Cantrill SJ, Turnbull WB, Stoddart JF (2005) *Acc Chem Res* 38:723
84. Balzani V, Credi A, Raymo FM, Stoddart JF (2000) *Angew Chem Int Ed* 39:3348
85. Sauvage J-P (1998) *Acc Chem Res* 31:611
86. Binnig G, Rohrer H (1987) *Rev Mod Phys* 59:615
87. Eigler DM, Schweizer EK (1990) *Nature* 344:524
88. Crommie MF, Lutz CP, Eigler DM (1993) *Science* 262:218
89. Avouris P (1995) *Acc Chem Res* 28:95
90. Gimzewski JK, Joachim C (1999) *Science* 283:1683
91. Hla S-W, Bartels L, Meyer G, Rieder K-H (2000) *Phys Rev Lett* 85:2777
92. Ho W (2002) *J Chem Phys* 117:11033
93. De Feyter S, De Schryver FC (2003) *Chem Soc Rev* 32:139
94. Barth JV, Weckesser J, Lin N, Dmitriev S, Kern K (2003) *Appl Phys A* 76:645
95. Barth JV, Costantini G, Kern K (2005) *Nature* 437:671
96. De Feyter S, De Schryver FC (2005) *J Phys Chem B* 109:4290
97. Wan L-J (2006) *Acc Chem Res* 39:334
98. Böhrringer M, Morgenstern K, Schneider W-D, Berndt R, Mauri F, Vita AD, Car R (1999) *Phys Rev Lett* 83:324
99. Yokoyama T, Yokoyama S, Kamikado T, Okuno Y, Mashiko S (2001) *Nature* 413:619
100. Schlickum U, Decker R, Klappenberger F, Zoppellaro G, Klyatskaya S, Auwärter W, Nepl S, Kern K, Brune H, Ruben M, Barth JV (2008) *J Am Chem Soc* (in press)
101. Barth JV, Weckesser J, Cai C, Günter P, Bürgi L, Jeandupeux O, Kern K (2000) *Angew Chem Int Ed* 39:1230
102. Barth JV, Weckesser J, Trimarchi G, Vladimirova M, Vita AD, Cai C, Brune H, Günter P, Kern K (2002) *J Am Chem Soc* 124:7991
103. Theobald JA, Oxtoby NS, Phillips MA, Champness NR, Beton PH (2003) *Nature* 424:1029
104. Stöhr M, Wahl M, Galka CH, Riehm T, Jung TA, Gade LH (2005) *Angew Chem Int Ed* 44:7394
105. Cañas-Ventura ME, Xiao W, Wasserfallen D, Müllen K, Brune H, Barth JV, Fasel R (2007) *Angew Chem Int Ed* 46:1814
106. Schiffrin A, Riemann A, Auwärter W, Pennec Y, Weber-Bargioni A, Cvetko D, Cosaro A, Morgante A, Barth JV (2007) *Proc Natl Acad Sci USA* 104:5279
107. Semenov A, Spatz JP, Möller M, Lehn J-M, Sell B, Schubert D, Weidl CH, Schubert US (1999) *Angew Chem Int Ed* 38:2547
108. Bernhard S, Takada K, Díaz DJ, Abruña HD, Mürner H (2001) *J Am Chem Soc* 123:10265
109. Kurth DG, Severin N, Rabe JP (2002) *Angew Chem Int Ed* 41:3681
110. Lin N, Dmitriev A, Weckesser J, Barth JV, Kern K (2002) *Angew Chem Int Ed* 41:4779
111. Messina P, Dmitriev A, Lin N, Spillmann H, Abel M, Barth JV, Kern K (2002) *J Am Chem Soc* 124:14000
112. Abdel-Mottaleb MMS, Schuurmans N, Feyter SD, Esch JV, Feringa BL, Schryver FCD (2002) *Chem Commun*, p 1894

113. Dmitriev A, Spillmann H, Lin N, Barth JV, Kern K (2003) *Angew Chem Int Ed* 41:2670
114. Spillmann H, Dmitriev A, Lin N, Messina P, Barth JV, Kern K (2003) *J Am Chem Soc* 125:10725
115. Stepanow S, Lingenfelder M, Dmitriev A, Spillmann H, Delvigne E, Lin N, Deng X, Cai C, Barth JV, Kern K (2004) *Nat Mater* 3:229
116. Safarowsky C, Merz L, Rang A, Broekmann P, Hermann BA, Schalley CA (2004) *Angew Chem Int Ed* 43:1291
117. De Feyter S, Abdel-Mottaleb MMS, Schuurmans N, Verkuijl B, Esch Jv, Feringa BL, De Schryver FC (2004) *Chem Eur J* 10:1124
118. Ruben M, Rojo J, Romero-Salguero FJ, Uppadine LH, Lehn J-M (2004) *Angew Chem Int Ed* 43:3644
119. Alam MS, Strömsdörfer S, Dremov S, Müller P, Kortus J, Ruben M, Lehn J-M (2005) *Angew Chem Int Ed* 44:7896
120. Clair S, Pons S, Brune H, Kern K, Barth JV (2005) *Angew Chem Int Ed* 44:7294
121. Clair S, Pons S, Fabris S, Baroni S, Brune H, Kern K, Barth JV (2006) *J Phys Chem B* 110:5627
122. Stepanow S, Lin N, Payer D, Schlickum U, Klappenberger F, Zoppellaro G, Ruben M, Brune H, Barth JV, Kern K (2007) *Angew Chem Int Ed* 46:710
123. Barth JV (2007) *Annu Rev Phys Chem* 58:375
124. Schlickum U, Decker R, Klappenberger F, Zoppellaro G, Klyatskaya S, Ruben M, Silanes I, Arnau A, Kern K, Brune H, Barth JV (2007) *Nano Lett* 7:3813
125. Zhao A, Li Q, Chen L, Xiang H, Wang W, Pan S, Wang B, Xiao X, Yang J, Hou JG, Zhu Q (2005) *Science* 309:1542
126. Iancu V, Deshpande A, Hla S-W (2006) *Nano Lett* 6:820
127. Wende H, Bernien M, Sorg C, Ponpandian N, Kurde J, Miguel J, Piantek M, Xu X, Eckhold P, Kuch W, Baberschke K, Panchmatia PM, Sanyal B, Oppenheimer RM, Eriksson O (2007) *Nat Mater* 6:516
128. Stepanow S, Lin N, Barth JV (2008) *J Phys Cond Matter* 20:184002
129. Dmitriev A, Lin N, Weckesser J, Barth JV, Kern K (2002) *J Phys Chem B* 106:6907
130. Stepanow S, Strunskus T, Lingenfelder M, Dmitriev A, Spillmann H, Lin N, Barth JV, Wöll C, Kern K (2004) *J Phys Chem B* 108:19392
131. Cañas-Ventura ME, Klappenberger F, Clair S, Pons S, Brune H, Kern K, Strunskus T, Wöll C, Fasel R, Barth JV (2006) *J Chem Phys* 125:184710
132. Donhauser ZJ, Mantoosh BA, Kelly KE, Bumm LA, Monnell JD, Stapleton JJ Jr, Rawlett AM, Allara DL, Tour JM, Weiss PS (2001) *Science* 292:2303
133. Castonguay M, Roy J-R, Rochefort A, McBreen PH (2000) *J Am Chem Soc* 122:518
134. Yokoyama T, Kamikado T, Yokoyama S, Mashiko S (2004) *J Chem Phys* 121:11993
135. Dmitriev A, Seitsonen AP, Spillmann H, Lin N, Strunskus T, Wöll C, Barth JV, Kern K (2006) *ChemPhysChem* 7:2197
136. Klappenberger F, Cañas-Ventura ME, Clair S, Pons S, Schlickum U, Kern K, Brune H, Qiu Z-R, Ruben M, Strunskus T, Wöll C, Fasel R, Comisso A, Vita AD, Barth JV (2007) *ChemPhysChem* 8:1782
137. Tomba G, Lingenfelder M, Costantini G, Kern K, Klappenberger F, Barth JV, Colombi Ciacchi L, De Vita A (2007) *J Phys Chem A* 111:12740
138. Auwärter W, Klappenberger F, Weber-Bargioni A, Schiffrin A, Strunskus T, Wöll C, Pennec Y, Schiffrin A, Riemann A, Barth JV (2007) *J Am Chem Soc* 129:11279
139. Romaner L, Heimel G, Brédas J-L, Gerlach A, Schreiber F, Johnson RL, Zegenhagen J, Duhm S, Koch N, Zojer E (2007) *Phys Rev Lett* 99:256801

140. Weber-Bargioni A, Auwärter W, Klappenberger F, Reichert J, Lefrançois S, Strunskus T, Wöll C, Schiffrin A, Pennec Y, Barth JV (2008) *ChemPhysChem* 9:89
141. Barth JV (2000) *Surf Sci Rep* 40:75
142. Brune H (1998) *Surf Sci Rep* 31:121
143. Barth JV (2006) In: Grütter P, Hofer W, Rosei F (eds) *Properties of single molecules on crystal surfaces*. World Scientific, Singapore
144. Nielsen LP, Besenbacher F, Stensgaard I, Lægsgaard E, Engdahl C, Stoltze P, Jacobsen KW, Nørskov JK (1993) *Phys Rev Lett* 71:754
145. Chambliss DD, Johnson KE (1994) *Phys Rev B* 50:5012
146. Barth JV, Behm RJ, Ertl G (1995) *Surf Sci* 341:62
147. Fischer B, Barth JV, Fricke A, Nedelmann L, Kern K (1997) *Surf Sci* 389:366
148. Besenbacher F, Chorkendorff I, Clausen BS, Hammer B, Molenbroek AM, Nørskov JK, Stensgaard I (1998) *Science* 279:1913
149. Ruben M (2005) *Angew Chem Int Ed* 44:1594
150. Ruben M, Lehn J-M, Müller P (2006) *Chem Soc Rev* 35:1056
151. Safarowsky C, Rang A, Schalley CA, Wandelt K, Broekmann P (2005) *Electrochim Acta* 50:4257
152. Gong JR, Wan LJ, Yuan QH, Bai CL, Jude H, Stang PJ (2005) *Proc Natl Acad Sci USA* 102:971
153. Nagy G, Mayer D, Wandlowski T (2002) *Phys Chem Commun* 5:112
154. Tao NJ (2006) *Nat Nanotechnol* 1:173
155. Wang D, Wan L-J (2007) *J Phys Chem C* 111:16109
156. Auwärter W, Weber-Bargioni A, Brink S, Riemann A, Schiffrin A, Ruben M, Barth JV (2007) *ChemPhysChem* 8:250
157. Shubina TE, Marbach H, Flechtner K, Kretschmann A, Jux N, Buchner F, Steinrück H-P, Clark T, Gottfried JM (2007) *J Am Chem Soc* 129:9476
158. Weber-Bargioni A, Reichert J, Seitsonen AP, Auwärter W, Schiffrin A, Barth JV (2008) *J Phys Chem C* 112:3453
159. Lu X, Hipps KW, Wang XD, Mazur U (1996) *J Am Chem Soc* 118:7190
160. Drain CM (2002) *Proc Natl Acad Sci USA* 99:5178
161. Milic TN, Chi N, Yablon DG, Flynn GW, Batteas JD, Drain CM (2002) *Angew Chem Int Ed* 41:2117
162. Hipps KW, Scudiero L, Barlow DE, Cooke MP (2002) *J Am Chem Soc* 124:2126
163. Bonifazi D, Spillmann H, Kiebele A, Wild Md, Seiler P, Cheng F, Güntherodt H-J, Jung T, Diederich F (2004) *Angew Chem Int Ed* 43:4759
164. Suto K, Yoshimoto S, Itaya K (2006) *Langmuir* 22:10766
165. Leung K, Rempe SB, Schultz PA, Sproviero EM, Batista VS, Chandross ME, Medforth CJ (2006) *J Am Chem Soc* 128:3659
166. Vaughan OPH, Williams FJ, Bampos N, Lambert RM (2006) *Angew Chem Int Ed* 45:3779
167. Auwärter W, Weber-Bargioni A, Schiffrin A, Riemann A, Gröning O, Fasel R, Barth JV (2006) *J Chem Phys* 124:194708
168. Auwärter W, Schiffrin A, Riemann A, Weber-Bargioni A, Pennec Y, Barth JV (2008) *Int J Nanotechnol* 5:1171
169. Lukasczyk T, Flechtner K, Merte LR, Jux N, Maier F, Gottfried JM, Steinrück H-P (2007) *J Phys Chem C* 111:3090
170. Lensen MC, Elemans JAAW, van Dingenen SJT, Gerritsen JW, Speller S, Rowan AE, Nolte RJM (2007) *Chem Eur J* 13:7948
171. Flechtner K, Kretschmann A, Bradshaw LR, Walz M-M, Steinrück H-P, Gottfried JM (2007) *J Phys Chem C* 111:5821

172. Yoshimoto S, Itaya K (2007) *J Porph Phthaloc* 11:313
173. Grillo SE, Tang H, Coudret C, Gauthier S (2002) *Chem Phys Lett* 355:289
174. Gersen H, Schaub R, Xu W, Stensgaard I, Laegsgaard E, Linderroth TR, Besenbacher F, Nazeeruddin MK, Grätzel M (2006) *Appl Phys Lett* 89:264102
175. Xu W, Dong M, Vázquez-Campos S, Gersen H, Lægsgaard E, Stensgaard I, Crego-Calama M, Reinhoudt DN, Linderroth TR, Besenbacher F (2007) *J Am Chem Soc* 129:10625
176. Tanaka H, Kawai T (1997) *J Vac Sci Technol B* 15:602
177. Yamada T, Suzuki H, Hidenori S, Mashiko S (2004) *J Natl Inst Inf Commun Technol* 51:111
178. Suzuki H, Yamada T, Kamikado T, Okuno Y, Mashiko S (2005) *J Phys Chem B* 109:13296
179. Okabayashi Y, Kanai K, Ouchi Y, Seki K (2006) *Rev Sci Instrum* 77:033905
180. Rader HJ, Rouhanipour A, Talarico AM, Palermo V, Samori P, Müllen K (2006) *Nat Mater* 5:276
181. Swarbrick JC, Ben Taylor J, O'Shea JN (2006) *Appl Surf Sci* 252:5622
182. Payer D, Rauschenbach S, Malinowski N, Konuma M, Virojanadara C, Starke U, Dietrich-Buchecker C, Collin J-P, Sauvage J-P, Lin N, Kern K (2007) *J Am Chem Soc* 129:15662
183. Guo S, Kandel SA (2008) *J Chem Phys* 128:014702
184. Shoji O, Tanaka H, Kawai T, Kobuke Y (2005) *J Am Chem Soc* 127:8598
185. Repp J, Meyer G, Paavilainen S, Olsson FE, Persson M (2006) *Science* 312:1196
186. Weber-Bargioni A (2007) PhD thesis, UBC Vancouver
187. Breitruck A, Hoster HE, Meier C, Ziener U, Behm RJ (2007) *Surf Sci* 601:4200
188. Lin N, Langner A, Tait SL, Rajadurai C, Ruben M, Kern K (2007) *Chem Commun*, p 4860
189. Matena M, Riehm T, Stöhr M, Jung TA, Gade LH (2008) *Angew Chem Int Ed* 47:2414
190. Frederick BG, Leibsle FM, Haq S, Richardson NV (2000) *Surf Rev Lett* 409:512
191. Perry CC, Haq S, Frederick BG, Richardson NV (1998) *Surf Sci* 409:512
192. Chen Q, Perry CC, Frederick BG, Murray PW, Haq S, Richardson NV (2000) *Surf Sci* 446:63
193. Giessen M (2001) *Prog Surf Sci* 68:1
194. Pascual JI, Barth JV, Ceballos G, Trimarchi G, De Vita A, Kern K, Rust H-P (2004) *J Chem Phys* 120:11367
195. Lin N, Payer D, Dmitriev A, Strunskus T, Wöll C, Barth JV, Kern K (2005) *Angew Chem Int Ed* 44:1488
196. Payer D, Comisso A, Dmitriev A, Strunskus T, Lin N, Wöll C, DeVita A, Barth JV, Kern K (2007) *Chem Eur J* 13:3900
197. Lingenfelder M, Spillmann H, Dmitriev A, Stepanow S, Lin N, Barth JV, Kern K (2004) *Chem Eur J* 10:1913
198. Stepanow S, Lin N, Vidal F, Landa A, Ruben M, Barth JV, Kern K (2005) *Nano Lett* 5:901
199. Vidal F, Delvigne E, Stepanow S, Lin N, Barth JV, Kern K (2005) *J Am Chem Soc* 127:10101
200. Meot-Ner M (2005) *Chem Rev* 105:213
201. Dmitriev A, Spillmann H, Lingenfelder M, Lin N, Barth JV, Kern K (2004) *Langmuir* 41:4799
202. Tait SL, Wang Y, Lin N, Costantini G, Baraldi A, Esch F, Petaccia L, Lizzit S, Kern K (2008) *J Am Chem Soc* 130:2108

203. Classen T, Fratesi G, Costantini G, Fabris S, Stadler FL, Kim C, Gironcoli SD, Baroni S, Kern K (2005) *Angew Chem Int Ed* 44:6142
204. Tait SL, Langner A, Lin N, Stepanow S, Rajadurai C, Ruben M, Kern K (2007) *J Phys Chem C* 111:10982
205. Pennec Y, Auwärter W, Schiffrin A, Weber-Bargione A, Barth JV (2007) *Nat Nanotechnol* 2:99
206. Wegner D, Yamachika R, Wang Y, Brar VW, Bartlett BM, Long JR, Crommie MF (2008) *Nano Lett* 8:131
207. Stepanow S, Lin N, Barth JV, Kern K (2006) *J Phys Chem B* 110:23472
208. Zhang Y-F, Zhu N, Komeda T (2007) *J Phys Chem C* 111:16946
209. Lin N, Stepanow S, Vidal F, Kern K, Alam MS, Strömsdörfer S, Dremov V, Müller P, Landa A, Ruben M (2006) *Dalton Trans*, p 2794
210. Lin N, Stepanow S, Vidal F, Barth JV, Kern K (2005) *Chem Commun*, p 1681
211. Langner A, Tait SL, Lin N, Rajadurai C, Ruben M, Kern K (2007) *Proc Natl Acad Sci USA* 104:17927
212. Fehllhammer WP, Fritz M (1993) *Chem Rev* 93:1243
213. Przychodzen P, Korzeniak T, Podgajny R, Sieklucka B (2006) *Coord Chem Rev* 250:2234
214. Decker R (2008) PhD thesis, EPF Lausanne
215. Hooks DE, Fritz T, Ward MD (2001) *Adv Mater* 13:227
216. Clair S, Pons S, Seitsonen AP, Brune H, Kern K, Barth JV (2004) *J Phys Chem B* 108:19392
217. Barth JV, Brune H, Ertl G, Behm RJ (1990) *Phys Rev B* 42:9307
218. Mendez J, Caillard R, Otero G, Nicoara N, Martin-Gago J (2006) *Adv Mater* 18:2048
219. Grant AG, Jones TE, Baddeley CJ (2007) *J Phys Chem C* 111:10534
220. Zhang Y-F, Zhu N, Komeda T (2008) *Surf Sci* 602:614
221. Stepanow S, Lin N, Barth JV, Kern K (2006) *Chem Commun*, p 2153
222. Seitsonen AP, Lingensfelder M, Spillmann H, Dmitriev A, Stepanow S, Lin N, Kern K, Barth JV (2006) *J Am Chem Soc* 126:5634
223. Zotti LA, Teobaldi G, Hofer WA, Auwärter W, Weber-Bargioni A, Barth JV (2007) *Surf Sci* 601:2409
224. Peng G, Elp Jv, Jang H, Que L, Armstrong WH, Cramer SP (1995) *J Am Chem Soc* 117:2515
225. Gao L, Ji W, Hu YB, Cheng ZH, Deng ZT, Liu Q, Jiang N, Lin X, Guo W, Du SX, Hofer WA, Xie XC, Gao H-J (2007) *Phys Rev Lett* 99:106402
226. Dubois LH, Nuzzo RG (1992) *Annu Rev Phys Chem* 43:437
227. Ulman A (1996) *Chem Rev* 96:1533
228. Yang HC, Aoki K, Hong H-G, Sackett DD, Arendt MF, Yau S-L, Bell CM, Mallouk TE (1993) *J Am Chem Soc* 115:11855
229. Hatzor A, Moav T, Cohen H, Matlis S, Libman J, Vaskevich A, Shanzer A, Rubinstein I (1998) *J Am Chem Soc* 120:13469
230. Haga M-A, Kobayashi K, Terada K (2007) *Coord Chem Rev* 251:2688
231. Uosaki K, Kondo T, Zhang X-Q, Yanagida M (1997) *J Am Chem Soc* 119:8367
232. Lin C, Kagan CR (2003) *J Am Chem Soc* 125:336
233. Ashkenazy G, Cahen D, Cohen R, Shanzer A, Vilan A (2002) *Acc Chem Res* 35:121
234. Menozzi E, Pinalli R, Speets EA, Ravoo BJ, Dalcanale E, Reinhoudt DN (2004) *Chem Eur J* 10:2199
235. Biemmi E, Scherb C, Bein T (2007) *J Am Chem Soc* 127:8054
236. Shekhah O, Wang H, Kowarik S, Schreiber F, Paulus M, Tolan M, Sternemann C, Evers F, Zacher D, Fischer RA, Wöll C (2007) *J Am Chem Soc* 129:15118

237. Crespo-Biel O, Ravoo BJ, Reinhoudt DN, Huuskens J (2006) *J Mater Chem* 16:3997
238. Pirondini L, Stendardo AG, Geremia S, Campagnolo M, Samori P, Rabe JP, Fokkens R, Dalcanale E (2003) *Angew Chem Int Ed* 42:1384
239. Surin M, Samori P, Jouaiti A, Kyritsakan N, Housseini MW (2007) *Angew Chem Int Ed* 46:245
240. Figgemeier E, Merz L, Hermann BA, Zimmermann YC, Housecroft CE, Güntherodt H-J, Constable EC (2003) *J Phys Chem B* 107:1157
241. Díaz DJ, Storrier GD, Bernhard S, Takada K, Abruña HD (1999) *Langmuir* 15:7351
242. Díaz DJ, Bernhard S, Storrier GD, Abruña HD (2001) *J Phys Chem B* 105:8746
243. Räisänen MT, Mögele F, Feodorow S, Rieger B, Ziener U, Leskelä M, Repo T (2007) *Eur J Inorg Chem*, p 4028
244. Newkome GR, Wang P, Moorefield CN, Cho TJ, Mohapatra PP, Li S, Hwang S-H, Lukoyanova O, Echegoyen L, Palagallo JA, Iancu V, Hla S-W (2006) *Science* 312:1782
245. Jeong KS, Kim SY, Shin U-S, Kogej M, Hai NTM, Broekmann P, Jeong N, Kirchner B, Reiher M, Schalley CA (2005) *J Am Chem Soc* 127:17672
246. Yuan Q-H, Wan L-J, Jude H, Stang PJ (2005) *J Am Chem Soc* 127:16279
247. Li S-S, Yan H-J, Wan L-J, Yang H-B, Northrop BH, Stang PJ (2007) *J Am Chem Soc* 129:9268
248. Yuan Q-H, Wan L-J (2006) *Chem Eur J* 12:2808
249. Ziener U, Lehn J-M, Mourran A, Möller M (2002) *Chem Eur J* 8:951
250. Weeks L, Thompson LK, Shapter JG, Pope KJ, Xu Z (2003) *J Microsc* 212:102
251. Milway VA, Abedin SMT, Niel V, Kelly TL, Dawe LN, Dey SK, Thompson DW, Miller DO, Alam MS, Müller P, Thompson LK (2006) *Dalton Trans*, p 2835
252. Wang Z, Deng Q, Luan Y, Wu X, Wan L, Wang C, Lee GU, Yin S, Yang J, Bai C (2003) *J Phys Chem B* 107:13384
253. Borrás-Almenar JJ, Coronado E, Müller A, Pope MT (2004) *Polyoxometalate molecular science*. Kluwer, Dordrecht
254. Pope MT, Müller A (2001) *Polyoxometalate chemistry: from topology via self-assembly to applications*. Kluwer, Dordrecht
255. Mal SS, Kortz U (2005) *Angew Chem Int Ed* 44:3777
256. Alam MS, Dremov V, Müller P, Postnikov A, Mal SB, Hussain F, Korz U (2006) *Inorg Chem* 45:2866
257. Tominaga M, Suzuki K, Kawano M, Kusukawa T, Ozeki T, Sakamoto S, Yamaguchi K, Fujita M (2004) *Angew Chem Int Ed* 43:5621
258. Busi M, Laurenti M, Condorelli GG, Motta A, Favazza M, Fragalà IL, Montalti M, Prodi L, Dalcanale E (2007) *Chem Eur J* 13:6891
259. Liu Y, Zhao Y-L, Zhang H-Y, Song H-B (2003) *Angew Chem Int Ed* 42:3260
260. Mateo-Marti E, Welte L, Ama-Ochoa P, Sanz Miguel PJ, Gómez-Herrero J, Martín-Gago JA, Zamora F (2008) *Chem Commun*, p 945
261. Novokmet S, Alam MS, Dremov V, Heinemann FW, Müller P, Alsfasser R (2005) *Angew Chem Int Ed* 44:803
262. Olea D, González-Prieto R, Priego JL, Carmen Barral M, de Pablo PJ, Rosario Torres M, Gómez-Herrero J, Jiménez-Aparicio R, Zamora F (2007) *Chem Commun*, p 1591
263. Zhang HM, Zhao W, Xie Z-X, Long L-S, Mao B-W, Xu X, Zheng L-S (2007) *J Phys Chem C* 111:7570